Complete set of polarization observables in $\vec{p}\vec{p} \rightarrow pp\pi^0$ close to threshold

H. O. Meyer,* A. Wellinghausen, J. T. Balewski, J. Doskow, R. E. Pollock, B. v. Przewoski, T. Rinckel, and P. Thörngren-Engblom†
Indiana University Cyclotron Facility, Bloomington, Indiana 47405

L. D. Knutson, W. Haeberli, B. Lorentz,‡ F. Rathmann,§ B. Schwartz, and T. Wise
Department of Physics, University of Wisconsin-Madison, Madison, Wisconsin 53706

W. W. Daehnick and Swapan K. Saha‖
Department of Physics and Astronomy, University of Pittsburgh, Pittsburgh, Pennsylvania 15260

P. V. Pancella
Department of Physics, Western Michigan University, Kalamazoo, Michigan 49008
(Received 5 January 2001; published 2 May 2001)

In a kinematically complete experiment we have measured the two analyzing powers and the five spin correlation coefficients of the reaction $\vec{p}\vec{p} \rightarrow pp\pi^0$ as a function of all five parameters of the three-body final state for bombarding energies between 325 and 400 MeV. The data are in disagreement with the theoretical predictions available at this time. Below 400 MeV, fewer than a dozen complex partial-wave amplitudes are likely to be significant, and it is expected that the present experimental information constrains these amplitudes. We also describe the formalism for an expansion of the spin observables into a complete set of angular functions and use this to completely characterize the polarization information obtainable from reactions with polarized spin-1/2 collision partners and a three-body final state.

DOI: 10.1103/PhysRevC.63.064002 PACS number(s): 24.70.+s, 24.80.+y, 25.10.+s, 29.20.Dh

I. INTRODUCTION

The behavior of a system consisting of two nucleons and a pion is basic to classical nuclear physics. It is thus an important task to try to relate the process of pion production in a nucleon-nucleon (NN) collision to our understanding of the NN interaction or to constraints given by basic symmetries, or, ultimately, to a model that features the constituents of nucleons and mesons. The theoretical task was expected to be relatively simple at energies very close to threshold because only a single angular momentum channel contributes.

Triggered by the advent of new cross section data close to threshold, there has been a flurry of theoretical activity during the past five years devoted to an understanding of the lowest partial wave (see Sec. V A for more details on the current status of the theory). Even though this work is still going on, it is clearly important to also investigate the higher partial waves which become active as the bombarding energy is increased. In order to identify the role of individual partial waves, the use of polarized collision partners is essential.

Each of the three periods of activity in the study of pion production in the nucleon-nucleon system is related to specific technical advances. The first was the development of accelerators with sufficient energy, which led to the first observation of the $pp \rightarrow pp\pi^0$ reaction [1] just a few years after the pion was discovered [2] and 17 years after it was predicted by Yukawa [3]. The second was the construction of meson factories with intense, well-defined proton beams that made possible accurate and kinematically complete cross section measurements, and the third was the advent of storage rings with electron-cooled beams and internal targets [4], which started to operate in the late 1980s, and which opened up the near-threshold region for experimental study.

Measurements of pion production in pp collisions benefit from storage ring technology mainly in two ways. The first concerns the use of windowless internal gas targets. Such targets put only hydrogen gas into the path of the beam and make it possible to measure small $pp \rightarrow pp\pi^0$ cross sections very close to threshold with little contamination from undesired reactions. In addition, the amount of material between the target volume and the detector can be made small, and the momenta of both outgoing hadrons can be measured accurately. Thus, the complete kinematics of each event can be determined. Internal targets must be thin in order for the cooling process to keep up with target heating, but this limitation is offset by the intensity of the accumulated, stored beam. The second unique advantage of the storage ring environment concerns polarized atomic gas targets. It turns out that the maximum target thickness that can be achieved is a good match for the target thickness requirements of a medium-energy storage ring.

Close to threshold the number of participating partial

*Email address: meyer@iucf.indiana.edu
†Present address: Department of Radiation Sciences, Uppsala University, Sweden.
‡Present address: Forschungszentrum Jülich, Germany.
§Present address: Universität Erlangen-Nürnberg, Erlangen, Germany.
‖Present address: Bose Institute, Calcutta, India.

 ©2001 The American Physical Society

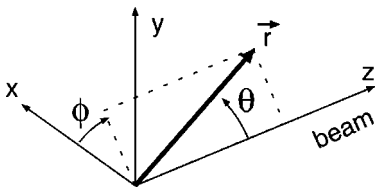

FIG. 1. Coordinate frame. The *z* axis is along the beam direction, the *y* axis is pointing up, and the *x* axis completes the right-handed coordinate system. The direction of a vector $\vec{r}$ is given by a polar angle θ and an azimuthal angle ϕ.

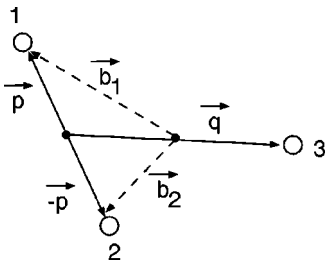

FIG. 2. The momenta and of the $pp \to pp\pi^0$ final state in the center-of-mass system. Particle numbers 1 and 2 are the two protons with momenta $\vec{b}_1$ and $\vec{b}_2$. The proton momentum in the pp rest system is given by $\vec{p}=(\vec{b}_1-\vec{b}_2)/2$ and the center-of-mass momentum of the pion (3) by $\vec{q}=-(\vec{b}_1+\vec{b}_2)$.

waves is small. In fact, at energies below 320 MeV, only one partial wave is significant (the **Ss** partial wave with the angular momenta of the final-state pp pair as well as the pion equal to zero). In one of the first nuclear physics experiments with a stored, cooled beam [5], the total cross section in this energy region was measured, revealing a serious disagreement with the theory at that time (see Sec. V A). For bombarding energies larger than 320 MeV, additional partial waves come into play but their number is still relatively small since below about 400 MeV final-state angular momenta larger than one should be unimportant. With this limitation, it is possible to provide an expression for the most general dependence of any observable on the angles of the three outgoing particles. For the present study, this point is crucial for two reasons. First, we use the angular dependence given by these expressions to formulate a strategy to order and present the information available from an experiment with polarized beam and target by defining an appropriate set of single-valued ''observables'' that characterize the complete five-dimensional phase space. Second, it allows us to carry out an analysis of the data in terms of the coefficients that appear in these expressions. The resulting coefficients completely parametrize the polarization observables of the reaction and constrain participating amplitudes individually. This constitutes a powerful and detailed test of any theory.

Prior to this experiment, the world's polarization data for the reaction $pp \to pp\pi^0$ below 400 MeV consisted of just two analyzing power measurements [6,7]. In this paper we describe a complete measurement of this reaction covering most of the available phase space, carried out with a polarized beam on a polarized target at bombarding energies between 325 and 400 MeV. All polarization observables allowed by parity conservation have been measured. Since we are dealing with a three-body final state, these observables depend on five kinematic variables. Section II of this paper is concerned with the definition of polarization observables and their dependence on the kinematics of the final state. Section III contains a description of the apparatus, an account of the acquired data, and a description of the method used to extract the observables from the measured quantities. In Sec. IV a scheme is introduced to completely map out the spin dependence of the reaction everywhere in the five-dimensional phase space, and results are presented. Finally, Sec. V is devoted to a discussion of the present status of the theory, a comparison of some of the data to recent calculations, and a list of conclusions from the present experiment.

II. POLARIZATION OBSERVABLES

A. Basic definitions

In a reaction with two outgoing particles it is customary to relate the coordinate frame to the reaction plane. With a three-body final state there is no such distinguished plane, so we use a Cartesian coordinate frame that is fixed in space. The *z* axis is along the beam direction, the *y* axis is vertical, pointing up, and the *x* axis completes the right-handed coordinate system. The polar angle θ and azimuthal angle ϕ, as defined in Fig. 1, are used to specify the direction of any vector.

In this experiment we detect the energy and direction of the two final-state protons of the reaction $pp \to pp\pi^0$. Let the center-of-mass momentum of the two protons be $\vec{b}_1$ and $\vec{b}_2$. To describe the final-state kinematics we define the momenta $\vec{p}$ and $\vec{q}$, where $\vec{p}=(\vec{b}_1-\vec{b}_2)/2$ (the proton momentum in the pp rest system) and $\vec{q}=-(\vec{b}_1+\vec{b}_2)$ (the center-of-mass momentum of the pion; see Fig. 2). Five independent parameters are needed to describe the final state, namely, the directions $\hat{p}$ and $\hat{q}$ and an ''energy-sharing'' parameter ϵ, which we will later define as the kinetic energy of the two final-state protons in their rest system [see Eq. (21)]. All five parameters follow from the observation of the two protons. For brevity, we sometimes denote the set $\{\theta_p, \varphi_p, \theta_q, \varphi_q, \epsilon\}$ by ξ.

The largest possible value of the pion momentum is given by (we set $c=\hbar=1$)

$$q_{\max}=\frac{1}{2\sqrt{s}}\sqrt{[s-(2m_p+m_\pi)^2][s-(2m_p-m_\pi)^2]}, \tag{1}$$

where $\sqrt{s}$ is the total center-of-mass energy, and m_p and m_π are the masses of the proton and the pion, respectively. Instead of the bombarding energy, one often quotes the parameter

$$\eta = q_{\max}/m_\pi, \tag{2}$$

which vanishes at threshold. The term ''near threshold'' loosely corresponds to the energy region with $\eta < 1$, i.e., below 400 MeV.

The polarization of an ensemble of spin-1/2 particles may be described by the expectation value of the three-component Pauli spin operator (see, e.g., Ref. [8]). In the following, we denote the polarization of the beam and the target by the two vectors $\vec{P} = (P_x, P_y, P_z)$ and $\vec{Q} = (Q_x, Q_y, Q_z)$, respectively.

B. Definition of observables

We abbreviate the differential cross section for the reaction, initiated by a polarized beam on a polarized target, by

$$\sigma(\xi, \vec{P}, \vec{Q}) \equiv \frac{d\sigma(\theta_p, \varphi_p, \theta_q, \varphi_q, \epsilon, \vec{P}, \vec{Q})}{d\Omega_p d\Omega_q d\epsilon}, \tag{3}$$

and write $\sigma_0(\xi)$ for the cross section that would be measured without polarization. In terms of the so-called Cartesian polarization observables, the spin-dependent cross section becomes

$$\sigma(\xi, \vec{P}, \vec{Q}) = \sigma_0(\xi) \cdot \Bigg[1 + \sum_i P_i A_{i0}(\xi) + \sum_j Q_j A_{0j}(\xi) + \sum_{i,j} P_i Q_j A_{ij}(\xi) \Bigg]. \tag{4}$$

Here, i and j stand for x, y, or z and the sums extend over all possibilities. The resulting 15 polarization observables include the beam analyzing powers A_{i0}, the target analyzing powers A_{0j}, and the spin correlation coefficients A_{ij}. It is convenient to define the following combinations of spin correlation coefficients:

$$A_\Sigma(\xi) \equiv A_{xx}(\xi) + A_{yy}(\xi), \tag{5a}$$

$$A_\Delta(\xi) \equiv A_{xx}(\xi) - A_{yy}(\xi), \tag{5b}$$

$$A_\Xi(\xi) \equiv A_{xy}(\xi) - A_{yx}(\xi). \tag{5c}$$

The 15 polarization observables of Eq. (4) are not independent. For instance, A_{x0} and A_{y0} are equivalent because the radiation pattern observed with a beam polarized along $\hat{y}$ is the same as when the beam is polarized along $\hat{x}$, except for a rotation by 90° around the z axis. This and other, similar, ''rotational'' equivalences are given by [9]

$$A_{x0}(\theta_p, \varphi_p, \theta_q, \varphi_q) = A_{y0}(\theta_p, \varphi_p + \pi/2, \theta_q, \varphi_q + \pi/2), \tag{6a}$$

$$A_{yz}(\theta_p, \varphi_p, \theta_q, \varphi_q) = A_{xz}(\theta_p, \varphi_p - \pi/2, \theta_q, \varphi_q - \pi/2), \tag{6b}$$

$$A_{xy}(\theta_p, \varphi_p, \theta_q, \varphi_q) + A_{yx}(\theta_p, \varphi_p, \theta_q, \varphi_q) = A_\Delta(\theta_p, \varphi_p - \pi/4, \theta_q, \varphi_q - \pi/4). \tag{6c}$$

If the two particles in the initial state are identical, measurements with interchanged beam and target polarization states must be equivalent. It is straightforward to show that if parity is conserved, the identity of the particles in the initial state requires

$$A_{ij}(\theta_p, \varphi_p, \theta_q, \varphi_q) = A_{ji}(\pi - \theta_p, \varphi_p + \pi, \pi - \theta_q, \varphi_q + \pi). \tag{7}$$

Applying the relations in Eqs. (5)–(7), we find that for the reaction $pp \to pp\pi^0$ there are the following seven independent polarization observables:

$$A_{y0}(\xi),\ A_{z0}(\xi),\ A_\Sigma(\xi),\ A_{zz}(\xi),\ A_{xz}(\xi),\ A_\Delta(\xi),\ A_\Xi(\xi). \tag{8}$$

The fact that the two nucleons in the final state are also identical requires that all observables must be invariant under the transformation $\vec{p} \to -\vec{p}$. This means that the phase space of the final state has two identical halves. In the analysis of the present experiment this is taken into account by always labeling the protons 1 and 2 in such a way that $0 \leqslant \theta_p \leqslant \pi/2$. Consequently, results are presented only for θ_p in this range, and when calculating a total cross section, the θ_p integral extends only from 0 to $\pi/2$.

For reactions with two colliding spin-1/2 particles, one can define three total cross sections, two of which depend on the spin. These total cross sections are related to the observables in Eq. (8) by

$$\sigma_{tot} = \int \sigma_0(\xi) d\Omega_p d\Omega_q d\epsilon, \tag{9a}$$

$$\Delta\sigma_T = -\int \sigma_0(\xi) A_\Sigma(\xi) d\Omega_p d\Omega_q d\epsilon, \tag{9b}$$

$$\Delta\sigma_L = -2\int \sigma_0(\xi) A_{zz}(\xi) d\Omega_p d\Omega_q d\epsilon, \tag{9c}$$

where $d\Omega = d\cos\theta d\varphi$, and the integration extends over $0 \leqslant \theta_q \leqslant \pi$, $0 \leqslant \theta_p \leqslant \pi/2$ and $0 \leqslant \epsilon \leqslant \epsilon_{\max}$. The possible value for $\Delta\sigma_L/\sigma_{tot}$ and $\Delta\sigma_T/\sigma_{tot}$ ranges between -2 and $+2$.

C. Angular momentum

1. Partial waves

Let us denote the angular momentum of the colliding protons by l, their channel spin by s_i, and the total angular momentum by J. In the final state, angular momentum, channel spin, and total angular momentum of the proton pair are given by l_p, s_f, and j, respectively, and the angular momentum of the (spinless) pion, relative to the center of mass, by l_q. This set of quantum numbers, denoted collectively by

$$\alpha=\{l,s_i,J,l_p,s_f,j,l_q\}, \tag{10}$$

fully identifies the amplitudes U_α for transitions from a given initial to a given final state. These amplitudes are functions of the energy-sharing parameter ϵ and the total energy. The quantum numbers in Eq. (10) are constrained by angular momentum and parity conservation as well as by the Pauli principle. Because close to threshold it is realistic to assume that l_p and l_q are either 0 or 1, the possible choices for the angular momentum in the final state are then $(l_p,l_q)=(0,0)$, (1,0), and (1,1), or **Ss**, **Ps**, and **Pp**. In $pp\rightarrow pp\pi^0$, there are *no* **Sp** final states permitted by the usual symmetry constraints of parity and angular momentum conservation and the Pauli principle. A list of all transitions with these constraints can be found in Table I. For completeness, we have included in Table I the transitions with $l_p=2$, $l_q=0$ (**Ds**) and $l_p=0$, $l_q=2$ (**Sd**). Since these amplitudes can interfere with the important **Ss** amplitude, their contribution might be non-negligible [10]. The list in Table I follows the conventional notation ${}^{2s_i+1}l_J\rightarrow{}^{2s_f+1}l_p,j,l_q$ where the spectroscopic notation, $(l,\ l_p)=S,\ P,\ D,\ F,\ \ldots$ and $l_q=s,\ p,\ d,\ f\ \ldots$ is used.

TABLE I. Angular momentum quantum numbers for the partial waves of the reaction $pp\rightarrow pp\pi^0$. The **Sd** and **Ds** amplitudes have been included for completeness sake; the present experiment finds no evidence for their significance.

Type	${}^{2s_i+1}l_J\rightarrow{}^{2s_f+1}l_{pj},l_q$
Ss	${}^3P_0\rightarrow{}^1S_0,s$
Ps	${}^1S_0\rightarrow{}^3P_0,s$
	${}^1D_2\rightarrow{}^3P_2,s$
Pp	${}^3P_0\rightarrow{}^3P_1,p$
	${}^3P_2\rightarrow{}^3P_1,p$
	${}^3P_2\rightarrow{}^3P_2,p$
	${}^3F_2\rightarrow{}^3P_1,p$
	${}^3F_2\rightarrow{}^3P_2,p$
	${}^3P_1\rightarrow{}^3P_0,p$
	${}^3P_1\rightarrow{}^3P_1,p$
	${}^3P_1\rightarrow{}^3P_2,p$
	${}^3F_3\rightarrow{}^3P_2,p$
Sd	${}^3P_2\rightarrow{}^1S_0,d$
	${}^3F_2\rightarrow{}^1S_0,d$
Ds	${}^3P_2\rightarrow{}^1D_2,s$
	${}^3F_2\rightarrow{}^1D_2,s$

2. Angular distributions of the observables

Since close to threshold only relatively few amplitudes contribute to $pp\rightarrow pp\pi^0$, it is feasible to expand the observables in terms of angular momentum. In the formalism we use, the expansion functions are products of two spherical harmonics with arguments $\hat{p}$ and $\hat{q}$, and the expansion coefficients are a sum of terms, where each term contains the product of two amplitudes $U_\alpha U^*_{\alpha'}$ times an angular-momentum coupling factor. The coupling factor is often zero, reflecting the constraints arising from conservation laws and antisymmetrization. For instance, one finds that the amplitudes can be arranged into the two groups (**Ss**, **Sd**, **Ds**) and (**Ps**, **Pp**), and only amplitudes within one group can interfere with each other. The details of such an expansion into partial waves are given in the Appendix.

Based on this partial-wave expansion, we have deduced equations that contain the dependence of the observables on the four angles that describe the final-state kinematics. The availability of such a set of equations is of crucial importance for the present work because it shows us how to analyze the measurement in view of the complexity of a five-dimensional phase space, and it guides us in defining a reasonable and complete set of observables that describes this complexity. It will be seen later that these equations provide a sufficient framework, since they are able to reproduce the measured angular distributions. The following set of equations represents the general angular dependence of the spin-averaged cross section $\sigma_0(\xi)$ and the spin dependent cross sections $\sigma_0(\xi)A_{ij}(\xi)$ in terms of the real coefficients E, F_k, G_k^{ij}, H_k^{ij}, I, and K. Note that we use $\Delta\varphi\equiv\varphi_p-\varphi_q$:

$$\sigma_0(\xi)=E+F_1+H_0^{00}+(H_1^{00}+I)(3\cos^2\theta_q-1)+(H_2^{00}+F_2+K)(3\cos^2\theta_p-1)+H_3^{00}(3\cos^2\theta_q-1)(3\cos^2\theta_p-1)$$
$$+H_4^{00}\sin 2\theta_p\sin 2\theta_q\cos\Delta\varphi+H_5^{00}\sin^2\theta_p\sin^2\theta_q\cos 2\Delta\varphi, \tag{11a}$$

$$\sigma_0(\xi)A_{y0}(\xi)=[\{G_1^{y0}+G_2^{y0}(3\cos^2\theta_p-1)\}\sin\theta_q+\{H_1^{y0}+I^{y0}+H_2^{y0}(3\cos^2\theta_p-1)\}\sin 2\theta_q]\cos\varphi_q$$
$$+[H_3^{y0}+K^{y0}+G_3^{y0}\cos\theta_q+H_4^{y0}(3\cos^2\theta_q-1)]\sin 2\theta_p\cos\varphi_p$$
$$+[G_4^{y0}\sin\theta_q+H_5^{y0}\sin 2\theta_q]\sin^2\theta_p\cos(2\varphi_p-\varphi_q)+H_6^{y0}\sin 2\theta_p\sin^2\theta_q\cos(2\varphi_q-\varphi_p), \tag{11b}$$

$$\sigma_0(\xi)A_\Sigma(\xi)=2(E-F_1)+H_0^\Sigma+(H_1^\Sigma+2I)(3\cos^2\theta_q-1)+(H_2^\Sigma-2F_2+2K)(3\cos^2\theta_p-1)+H_3^\Sigma(3\cos^2\theta_p-1)(3\cos^2\theta_q-1)$$
$$+H_4^\Sigma\sin 2\theta_p\sin 2\theta_q\cos\Delta\varphi+H_5^\Sigma\sin^2\theta_p\sin^2\theta_q\cos 2\Delta\varphi, \tag{11c}$$

$$\sigma_0(\xi)A_{zz}(\xi)=-E-F_1+H_0^{zz}+(H_1^{zz}-I)(3\cos^2\theta_q-1)+(H_2^{zz}-F_2-K)(3\cos^2\theta_p-1)+H_3^{zz}(3\cos^2\theta_p-1)(3\cos^2\theta_q-1)$$
$$+H_4^{zz}\sin 2\theta_p\sin 2\theta_q\cos\Delta\varphi+H_5^{zz}\sin^2\theta_p\sin^2\theta_q\cos 2\Delta\varphi, \tag{11d}$$

$$\sigma_0(\xi)A_\Delta(\xi)=[H_1^\Delta+H_2^\Delta(3\cos^2\theta_p-1)]\sin^2\theta_q\cos 2\varphi_q+[H_3^\Delta+H_4^\Delta(3\cos^2\theta_q-1)]\sin^2\theta_p\cos 2\varphi_p + H_5^\Delta\sin 2\theta_p\sin 2\theta_q\cos(\varphi_p+\varphi_q), \tag{11e}$$

$$\sigma_0(\xi)A_{xz}(\xi)=[\{G_1^{xz}+G_2^{xz}(3\cos^2\theta_p-1)\}\sin\theta_q+\{H_1^{xz}+I^{xz}+H_2^{xz}(3\cos^2\theta_p-1)\}\sin 2\theta_q]\cos\varphi_q + [H_3^{xz}+K^{xz}+G_3^{xz}\cos\theta_q+H_4^{xz}(3\cos^2\theta_q-1)]\sin 2\theta_p\cos\varphi_p + [G_4^{xz}\sin\theta_q+H_5^{xz}\sin 2\theta_q]\sin^2\theta_p\cos(2\varphi_p-\varphi_q)+H_6^{xz}\sin 2\theta_p\sin^2\theta_q\cos(2\varphi_q-\varphi_p), \tag{11f}$$

$$\sigma_0(\xi)A_{z0}(\xi)=[H_1^{z0}\sin 2\theta_q+G_1^{z0}\sin\theta_q]\sin 2\theta_p\sin\Delta\varphi+H_2^{z0}\sin^2\theta_p\sin^2\theta_q\sin 2\Delta\varphi, \tag{11g}$$

$$\sigma_0(\xi)A_\Xi(\xi)=G_1^\Xi\sin 2\theta_p\sin\theta_q\sin\Delta\varphi. \tag{11h}$$

The letter symbols E, F_k, G_k^{ij}, and H_k^{ij} distinguish terms with $(\mathbf{Ss})^2$, $(\mathbf{Ps})^2$, $(\mathbf{PsPp})$, and $(\mathbf{Pp})^2$ angular momenta in the final state according to the definitions given in Tables I and II. The superscript associates the coefficient with a given observable, and the subscript enumerates multiple occurrences of the same symbol within a given observable. A coefficient without a superscript appears in more than one observable. The coefficients I, K, I^{ij}, and K^{ij} are associated with **SsSd** or **SsDs** interference terms. We note that they always occur in conjunction with an H_k^{ij} term. Thus, the angular dependence alone does not provide sufficient information to separate the d-wave contributions. All contributions of the amplitudes listed in Table I have been taken into account, except those that correspond to a $(\mathbf{Ds})^2$ and $(\mathbf{Sd})^2$ final state.

The physics of the reaction is contained in the values of the coefficients E, F_k, G_k^{ij}, H_k^{ij}, I, and K. We will determine these values as a way to parametrize the results of the measurement. These coefficients are bilinear sums of the reaction amplitudes. The corresponding relations between the coefficients and the amplitudes are known, but often complicated. They can be derived from the partial-wave expansion described in the Appendix. Thus, in principle, it is possible to construct a set of amplitudes that best describes the present data; however, this task involves a nonlinear fit with a nondiagonal error matrix and possible ambiguities, and is beyond the scope of this paper.

TABLE II. Partial waves according to the final-state angular momenta. The column labeled L lists the symbol used in Eqs. (11) for a parameter of this type. The last column shows the power of η for the expected dependence on bombarding energy for the cases where neither l_p nor l_p' is zero.

Final-state angular momenta							
	l_p	l_q	l_p'	l_q'	L	$w_L(\epsilon)$	η^m
$(\mathrm{Ss})^2$	0	0	0	0	E	$q\cdot p\cdot f(\epsilon)\,d\epsilon$	-
$(\mathrm{Ps})^2$	1	0	1	0	F	$q\cdot p^3\,d\epsilon$	η^6
PsPp	1	0	1	1	G	$q^2\cdot p^3\,d\epsilon$	η^7
$(\mathrm{Pp})^2$	1	1	1	1	H	$q^3\cdot p^3\,d\epsilon$	η^8
SsSd	0	0	0	2	I	$q^3\cdot p\cdot f(\epsilon)\,d\epsilon$	-
SsDs	0	0	2	0	K	$q\cdot p^3\cdot\sqrt{f(\epsilon)}\,d\epsilon$	-

Equations (11) explicitly depend on the four angles θ_p, φ_p, θ_q, and φ_q, while the energy-sharing parameter ϵ is contained in the coefficients. A discussion of the energy dependence is given in Sec. IV E.

When calculating the value of a polarization observable from Eqs. (11), one has to evaluate the ratio $A_{ij}(\xi)=\sigma_0(\xi)A_{ij}(\xi)/\sigma_0(\xi)$, and an overall normalization of all terms in these equations cancels. Here, we choose to multiply all coefficients by $8\pi^2/\sigma_{tot}$. This makes the coefficients dimensionless. The spin-averaged total cross section is then an incoherent sum of the partial total cross sections $\sigma(Ss)/\sigma_{tot}=E$, $\sigma(Ps)/\sigma_{tot}=F_1$, and $\sigma(Pp)/\sigma_{tot}=H_0^{00}$, involving the three final states with $(\mathbf{Ss})^2$, $(\mathbf{Ps})^2$, and $(\mathbf{Pp})^2$, and

$$E+F_1+H_0^{00}=1. \tag{12a}$$

The spin-dependent total cross sections are then given by

$$\Delta\sigma_T/\sigma_{tot}=-2E+2F_1-H_0^\Sigma, \tag{12b}$$

$$\Delta\sigma_L/\sigma_{tot}=2E+2F_1-2H_0^{zz}. \tag{12c}$$

It should be noted that not all coefficients are independent. For instance, we know from the partial-wave analysis (see the Appendix) that for $m=0,\ldots,5$,

$$H_m^{00}=H_m^\Sigma+H_m^{zz} \tag{12d}$$

holds. Combining Eqs. (12b)–(12d) one easily derives the important relation

$$\frac{\sigma(Ps)}{\sigma_{tot}}=\frac{1}{4}\left(1+\frac{\Delta\sigma_T}{\sigma_{tot}}+\frac{1}{2}\frac{\Delta\sigma_L}{\sigma_{tot}}\right). \tag{13}$$

This relation, which holds for $pp\to pp\pi^0$, allows one to determine, in a model-independent way, the total strength of the reaction going to a **Ps** final state directly from the measured total cross sections. This *measurement of a partial wave* has been presented in an earlier publication [11], where the relation given in Eq. (13) appears without proof.

TABLE III. Bombarding energies used in this experiment, the η parameter [Eq. (2)], and the upper bound ϵ_{max} on the energy-sharing parameter [Eq. (21)]. Also listed are the accumulated luminosities and the products of beam and target polarization for the two phases of the experiment (see Sec. III B).

			Run A		Run B			
Energy (MeV)	η	ϵ_{max} (MeV)	$\int L\,dt$ (nb^{-1})	P_yQ	$\int L\,dt$ (nb^{-1})	P_xQ	P_yQ	P_zQ
325.6	0.560	21	2.163	0.456 (3)	3.0	0.059 (2)	0.333 (2)	0.296 (3)
350.5	0.707	33	0.901	0.342 (4)	1.3	0.053 (3)	0.316 (3)	0.267 (5)
375.0	0.832	44	3.024	0.514 (4)	4.1	0.041 (2)	0.333 (2)	0.266 (4)
400.0	0.948	55	0.831	0.526 (6)	1.1	0.039 (4)	0.289 (4)	0.203 (8)

III. MEASUREMENTS

A. Apparatus

The experiment was carried out with the Indiana Cooler storage ring. A detailed description of the apparatus has been presented previously in a technical paper [12]. In the following, we give an abbreviated description of the experimental setup, pointing out features that are especially important in appreciating the benefits and limitations of the technique employed.

1. Beam

A polarized 197 MeV proton beam from the IUCF cyclotron was accumulated in the Cooler ring, resulting in orbiting currents of 100–200 μA. The energy of the stored beam was then ramped to the desired value (for a list of energies, see Table III). The beam energy was known to better than 100 keV, and the polarization of the beam varied between 0.65 and 0.70.

The experiment was conducted in two phases. During the first phase, the beam polarization was vertical (along $\hat{y}$), while in the second phase nonvertical polarization was used. The latter is achieved with two spin-rotating solenoids. Their field is held fixed during acceleration. The field integral of these solenoids is limited, partly by the current limit of the solenoid, partly by difficulties in adjusting the ring optics to compensate for the additional focusing. The consequence of this limitation is that purely longitudinal beam polarization cannot be achieved for beam energies larger than 200 MeV. Instead, for the second phase of the experiment, the actual polarization direction is about $\vec{P}/P=(0.12,0.75,0.65)$, somewhat depending on beam energy (for actual values, see Table III).

The filling and ramping process takes 1–2 min, followed by 5–8 min of data taking. This beam cycle is then repeated. The sign of the beam polarization is changed every cycle.

2. Target

The stored beam passes through a target cell that consists of an open-ended 12 mm diameter cylindrical tube constructed from 25 μm aluminum foil. The tube is 25 cm long; the center of the cell defines the origin of the z axis. Joined to the side of this tube, at $z=0$, is a similar ''feed'' tube that is oriented towards the incident beam of polarized atoms. The target cell is supported by the end of the feed tube. It is possible to remotely adjust the cell position relative to the stored beam, in order to minimize the overlap between the beam halo and the cell wall. An atomic beam source [13] delivers the polarized hydrogen atoms. This source produces a beam of about 1 cm diameter with a flux of about 3×10^{16} atoms per second in a pure spin state with a nuclear polarization of about $Q=0.75$. The role of the target cell is to improve the utilization of the source output. The cell is coated with Teflon, which practically eliminates depolarization of the atoms during wall collisions. The total thickness of the target is a few times 10^{13} atoms/cm^2. The density of the target is determined by the gas flow through the cell, decreasing linearly from a maximum in the cell center to near zero at the open ends. The polarization direction is selected by a magnetic guide field of a few gauss in the region of the target. This field is generated by coils exterior to the scattering chamber, and can be oriented in the $\pm x$, $\pm y$, and $\pm z$ directions. It has been shown [14] that the magnitude of the target polarization does not vary significantly when the polarization direction is changed, and in the following we assume $Q=Q_x=Q_y=Q_z$ for the target polarization. During data acquisition the direction of the target polarization is changed every 2 s.

Internal polarized targets of this kind are pure and not susceptible to radiation damage, and they offer the possibility of rapidly changing the polarization direction.

3. Detector

The purpose of the detector is to measure the directions and energies of the two outgoing protons. This is accomplished with a stack of scintillators and wire chambers that are arranged as shown in Fig. 3. The directions of the two outgoing protons are determined by a set of four planes of wire chambers, and the ''E'' and the ''K'' scintillator arrays measure the energies of the protons.

The combined thickness of the E and the K detector planes is sufficient to stop the protons from the $pp\rightarrow pp\pi^0$ reaction for up to 400 MeV bombarding energy. The light from both planes is added and then converted to the energy of the stopped particle using a phenomenological expression for the light response, and a correction for the position-dependent light collection efficiency. The angular coverage of the detector depends on where along the target cell axis the event occurs. Seen from the center of the cell, the detec-

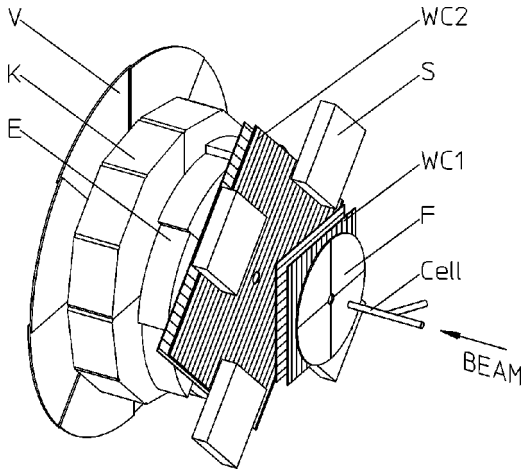

FIG. 3. Detector system to detect the two outgoing protons. The scintillators E and K measure energies and the wire chambers WC1 and WC2 directions. The scintillator V vetoes background events containing energetic charged particles. The four scintillators S provide a concurrent measurement of pp elastic scattering near $\theta_{lab} = 45°$ as a monitor for beam and target polarization. For more details see Sec. III A 3.

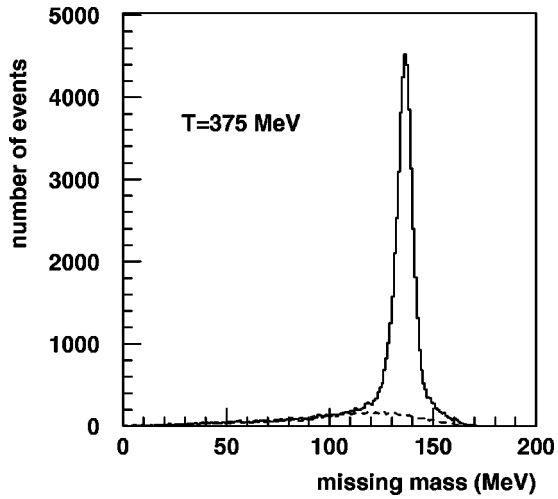

FIG. 4. Missing-mass spectrum of the $pp \rightarrow pp\pi^0$ reaction at 375 MeV. The dashed line shows the normalized background shape obtained with a N_2 target.

tor stack subtends a cone with a half-angle of 35°, with a 5° hole in the center that is required to admit the beam pipe for the circulating beam. This hole is responsible for most of the departure of the detector acceptance from 100%. The consequences of incomplete acceptance are discussed in Sec. IV F.

The wall of the vacuum chamber just downstream of the target consists of a 0.18-mm-thick, stainless steel window. A 1.5-mm-thick scintillator (''F'' in Fig. 3), immediately following this window, provides a start signal for a time-of-flight measurement for particle identification, and eliminates events originating in the beam pipe downstream of the F detector.

The E detector is divided into eight segments. The trigger for processing an event is a coincidence between the F detector and at least two segments of the E detector. A veto issued by the last scintillator in the stack (''V'' in Fig. 3) removes events where at least one particle is not stopped in either the E or the K scintillator, and thus are not from pion production.

Concurrent with the acquisition of $pp \rightarrow pp\pi^0$ events, pp elastic scattering is observed near $\theta_{lab} = 45°$ by four scintillators (labeled ''S'' in Fig. 3). For elastic scattering events a coincidence between two opposite detectors is required. Particles reaching the S detectors traverse the first set of wire chambers (''WC1'' in Fig. 3). A coplanarity condition and the known angle between the two protons provide a clean selection of pp elastic events.

B. Acquired data

The experiment has been conducted in two phases. In the first (called ''run A'') the beam polarization was vertical (along or opposite the y axis) and the target polarization was alternated in 2 s intervals between four directions (along or opposite the x axis or the y axis). Thus, data were accumulated with eight combinations of beam and target polarization (P_n, Q_m), namely, $(\pm P_y, \pm Q_x)$ and $(\pm P_y, \pm Q_y)$. Run A, which took place in the fall of 1997, was thus limited to observables that are accessible with only transverse polarization.

In the second phase (called ''run B''), spin rotators were employed to generate nonvertical beam polarization (see Sec. III A 1). In this case, the beam polarization was a sum of three components (P_x, P_y, P_z), and the target polarization was alternated between the six directions $\pm Q_x$, $\pm Q_y$, and $\pm Q_z$, giving rise to 12 different spin states $(\pm \vec{P}, \pm \vec{Q}_x)$, $(\pm \vec{P}, \pm \vec{Q}_y)$, and $(\pm \vec{P}, \pm \vec{Q}_z)$. Run B was carried out in the spring and fall of 1998. All possible analyzing powers and spin correlation coefficients were measured.

During both runs data were acquired at the beam energies 325, 350, 375, and 400 MeV. The respective integrated luminosities, together with the values for beam and target polarization, are listed in Table III.

C. Measured yields

1. Selecting the $pp \rightarrow pp\pi^0$ events

Events of interest are selected off line by requiring that both particles be identified as protons, that their wire chamber tracks be consistent with the patterns of responding segments in the various scintillator arrays, and that the origin of the event be in the target region. For each event the mass of the third, unobserved particle is calculated from the four-momenta of the two protons. An example of a missing mass spectrum is shown in Fig. 4. To accept an event, its missing mass has to be close to the mass of a neutral pion.

The amount of background under the pion mass peak varies with bombarding energy but is never larger than 10%. This background is caused by reactions of protons with the aluminum cell walls and with impurities in the target gas. Monte Carlo studies show that only reactions with three or more protons in the final state contribute significantly while

$(p,2p)$ reactions are unimportant. The shape of the background is determined from a separate measurement where the hydrogen in the target cell is replaced by N_2. This measurement results in a missing-mass spectrum that closely matches the one observed with a hydrogen target, except for the π^0 peak, and is therefore used to subtract the background under the pion peak.

The kinematics of the event is transformed to the center-of-mass system, and the angles θ_p, φ_p, θ_q, and φ_q as well as the energy-sharing parameter ϵ are calculated. For each accepted event, these parameters, together with information on the direction of the beam and target polarization at the time of the event, are stored for further processing.

2. Spin-dependent yields

We define the ''yield'' to be the number of events in a certain region $\Delta\xi$ of phase space, defined by conditions on the five kinematic variables ξ of the final state. There is one such yield $Y_{m,n}(\xi)$, for each combination (m,n) of beam and target polarization. For run A there are 8 and for run B 12 such combinations. The yields in different spin states are always background corrected and normalized such that they correspond to equal accumulated luminosity in every spin state. This normalization compensated differences of a few percent in the luminosity with different beam polarization. The integrated luminosity was determined from a concurrent measurement of pp elastic scattering (see next section).

3. Monitoring beam and target polarization and the luminosity

Concurrent with the measurement of pion production, elastic pp scattering is observed by a dedicated set of four detectors that covers the angular region near $\theta_{lab}=45°$. For these angles, the pp scattering spin correlation coefficients A_Δ and A_{zz} are quite large and well known [15]. This provides a sensitive on-line monitor for the products P_xQ_x, P_yQ_y, and P_zQ_z of all three beam polarization components and the target polarization $Q=Q_x=Q_y=Q_z$. Note that the pp elastic scattering analyzing powers near $\theta_{lab}=45°$ are small, so that the individual values for P and Q are not well determined from this measurement; however, these numbers are not needed for the subsequent analysis. From the pp scattering yield, averaged over azimuth and from the known cross section, we also deduce the integrated luminosity accumulated with each of the combinations of beam and target polarization. The relative luminosities are used to normalize the pion production yields in different spin states to equal integrated luminosity.

D. Asymmetries

From the spin-dependent yields, three different asymmetries can be calculated. The first, S_P, is the beam polarization asymmetry. It is obtained from the difference in the yields with positive and negative beam polarization, summed over all target polarization directions j:

$$S_P=\frac{\sum_{m=x,y,z}(Y_{+,Q_m}-Y_{-,Q_m})}{\sum_{m=x,y,z}(Y_{+,Q_m}+Y_{-,Q_m})}. \tag{14a}$$

Since each target orientation occurs with both signs, this effectively corresponds to an unpolarized target. The sum in the denominator is an average over both beam and target polarization direction, and thus represents the spin-averaged yield. Note that for run B the beam polarization is not along one of the coordinate axes and the asymmetry S_P contains contributions from all the three polarization components.

The three target polarization asymmetries for the target polarization directions $m = x$, y or z are given by

$$S_{Q_m}=\frac{\sum_{n=+,-}(Y_{n,+Q_m}-Y_{n,-Q_m})}{\sum_{n=+,-}(Y_{n,+Q_m}+Y_{n,-Q_m})}, \tag{14b}$$

where the sum over n provhdes the average over the beam polarization direction.

Finally, the three spin correlation asymmetries, again with the target polarization in the $m = x$, y, or z directions, are given by

$$S_{P,Q_m}=\frac{(Y_{+,+Q_m}+Y_{-,-Q_m})-(Y_{+,-Q_m}+Y_{-,+Q_m})}{(Y_{+,+Q_m}+Y_{-,-Q_m})+(Y_{+,-Q_m}+Y_{-,+Q_m})}. \tag{14c}$$

These asymmetries will be needed as a function of some of the kinematic variables ξ while integrating over the others. For instance, if we want to know the asymmetries as a function of θ_q and φ_q, we sort the events into bins that divide the full range of θ_q and φ_q to obtain the yields $Y_{n,m}(\theta_q,\varphi_q)$ while ignoring the other kinematic variables. If the detector acceptance is 100%, ignoring a kinematic variable is equivalent to integrating over that variable. Corrections due to incomplete detector acceptance are discussed in Sec. IV F. The asymmetries S_P, S_{Q_m}, and S_{P,Q_m} of Eq. (14) form the basis for deducing the observables as described in Secs. IV B and IV C.

IV. RESULTS

A. Exploring the five-dimensional phase space

The dependence of each polarization observable on five kinematic variables contains a wealth of detailed information about the reaction, but it also presents the difficulty of ordering and accessing this information. In the present case we benefit from the limited number of amplitudes, which permits us to determine the functional dependence of the observables on the angles θ_q, φ_q, θ_p, φ_p [Eq. (11)]. Based on this knowledge we now develop a procedure for extracting polarization information from the data in a systematic and complete way.

Inspecting Eq. (11), we note that the azimuthal functions $\Phi_k(\varphi_q,\varphi_p)$ that occur are one of the following: φ_q, φ_p, $\varphi_p+\varphi_q$, $2\varphi_p-\varphi_q$, $2\varphi_q-\varphi_p$, or $\varphi_p-\varphi_q$. Assume that we evaluate the asymmetries versus one of these functions Φ_k ($k=1,\ldots,6$) by sorting the events into bins of constant Φ_k. This is equivalent to an integral over azimuth with the condition $\Phi_k=$const, and eliminates one of the two azimuthal degrees of freedom. The implied integration retains only terms in Eqs. (11) that either contain Φ_k or do not depend on azimuth at all. To further reduce the remaining terms, we evaluate observables as a function of one of the polar angles θ (θ_p or θ_q), while integrating over the other one by ignoring it. Thus, for each of the polarization observables listed in Eq. (8), we have the choice of six azimuthal functions Φ_k and two polar angles. The resulting set of observables that are now functions of a single variable (either θ_p or θ_q) represents completely the effect of polarized collision partners on the angular variables. For now, we ignore the dependence on the energy-sharing parameter ϵ, and integrate over this quantity as well. The dependence on ϵ will be discussed separately in Sec. IV E.

B. A_{y0}, A_Σ, A_{zz}, A_Δ, and A_{xz}

The spin-dependent cross sections $\sigma_0 A_{y0}$, $\sigma_0 A_\Sigma$, $\sigma_0 A_{zz}$, $\sigma_0 A_\Delta$, and $\sigma_0 A_{xz}$ contain only terms that are either azimuth independent or proportional to $\cos\Phi_k$ or $\cos 2\Phi_k$ where Φ_k is one of five azimuthal dependences. Let us define the polarization observable $A_{ij}^{\Phi_k}(\theta_q)$ [or $A_{ij}^{\Phi_k}(\theta_p)$] as that part of the observable A_{ij} that remains when integrating over θ_p [or θ_q] and over φ_q and φ_p with the constraint $\Phi_k=0$. Of course, we still distinguish contributions with $\cos\Phi_k$ from those with $\cos 2\Phi_k$, since we have knowledge of the full Φ_k distribution. In this definition, the particular Φ_k selected is used as a superscript as a reminder that Φ_k is used to isolate the corresponding term; it no longer appears in the functional dependence of the observable. As an example, the transverse beam analyzing power that would be measured when observing just the pion, in the present notation, would be $A_{y0}^{\phi_q}(\theta_q)$. Using this definition, we end up with the following observables:

$$A_\Sigma(\theta_q),\quad A_\Sigma(\theta_p):\quad A_{zz}(\theta_q):\quad A_{zz}(\theta_p),$$

$$A_{y0}^{\varphi_q}(\theta_q),\quad A_{xz}^{\varphi_q}(\theta_q),\quad A_\Delta^{\varphi_q}(\theta_q),$$

$$A_{y0}^{\varphi_p}(\theta_p),\quad A_{xz}^{\varphi_p}(\theta_p),\quad A_\Delta^{\varphi_p}(\theta_p),$$

$$A_{y0}^{\varphi_p}(\theta_q),\quad A_{y0}^{2\varphi_p-\varphi_q}(\theta_q),\quad A_{y0}^{2\varphi_q-\varphi_p}(\theta_q),$$

$$A_{y0}^{\varphi_p}(\theta_p),\quad A_{y0}^{2\varphi_p-\varphi_q}(\theta_p),\quad A_{y0}^{2\varphi_q-\varphi_p}(\theta_p),$$

$$A_{xz}^{\varphi_p}(\theta_q),\quad A_{xz}^{2\varphi_p-\varphi_q}(\theta_q),\quad A_{xz}^{2\varphi_q-\varphi_p}(\theta_q),$$

$$A_{xz}^{\varphi_p}(\theta_p),\quad A_{xz}^{2\varphi_p-\varphi_q}(\theta_p),\quad A_{xz}^{2\varphi_q-\varphi_p}(\theta_p),$$

$$A_\Delta^{\varphi_p}(\theta_q),\quad A_\Delta^{\varphi_p+\varphi_q}(\theta_q),\quad A_\Delta^{\varphi_q}(\theta_p). \tag{15}$$

These 25 independent observables are extracted from the data as follows. First, we sort the events into bins for the selected polar angle $\theta=\theta_p$ or θ_q and azimuth function Φ_k to obtain the asymmetries $S_P(\theta,\Phi_k)$, $S_{Q_m}(\theta,\Phi_k)$, and $S_{P,Q_m}(\theta,\Phi_k)$ in Eq. (14). Next, we insert the spin-dependent cross section, Eq. (4), into the expression for the asymmetries. For instance, for the beam asymmetry [Eq. (14a)] this results in $S_P(\theta,\Phi_k)=P_x A_{x0}(\theta,\Phi_k)+P_y A_{y0}(\theta,\Phi_k)$. Similarly, Eq. (14b) yields the two relations $S_{Q_j}(\theta,\Phi_k)=QA_{0j}(\theta,\Phi_k)$, where $j=x$ or y. We then use the equivalences in Eqs. (6) and (7) and the definition of $A_{y0}^{\Phi_k}(\theta)$ to obtain

$$S_P(\theta,\Phi_k)=A_{y0}^{\Phi_k}(\theta)(P_y\cos\Phi_k-P_x\sin\Phi_k), \tag{16a}$$

$$S_{Q_x}(\theta,\Phi_k)=A_{y0}^{\Phi_k}(\theta)Q\sin\Phi_k, \tag{16b}$$

$$S_{Q_y}(\theta,\Phi_k)=A_{y0}^{\Phi_k}(\theta)Q\cos\Phi_k. \tag{16c}$$

The Φ_k distributions of the asymmetries on the left are measured. Since Eqs. (16) constrain the ratios P_y/Q and P_x/Q, knowing just the products P_xQ and P_yQ (see Sec. III C 3) is sufficient to extract $A_{y0}^{\Phi_k}(\theta)$.

In a similar fashion, the spin correlation observables are extracted; note that the observables A_Σ and A_{zz} have no azimuthal dependence, except for the terms containing $\Delta\varphi=\varphi_p-\varphi_q$ which will be discussed separately in the next section:

$$S_{P,Q_x}(\theta,\Phi_k)=1/2A_\Sigma(\theta)P_xQ+1/2A_\Delta^{\Phi_k}(\theta)(P_xQ\cos 2\Phi_k+P_yQ\sin 2\Phi_k)-A_{xz}^{\Phi_k}(\pi-\theta)P_zQ\cos\Phi_k, \tag{17a}$$

$$S_{P,Q_y}(\theta,\Phi_k)=1/2A_\Sigma(\theta)P_yQ+1/2A_\Delta^{\Phi_k}(\theta)(P_xQ\sin 2\Phi_k-P_yQ\cos 2\Phi_k)-A_{xz}^{\Phi_k}(\pi-\theta)P_zQ\sin\Phi_k, \tag{17b}$$

$$S_{P,Q_z}(\theta,\Phi_k)=A_{xz}^{\Phi_k}(\theta)(P_xQ\cos\Phi_k+P_yQ\sin\Phi_k)+A_{zz}(\theta)P_zQ. \tag{17c}$$

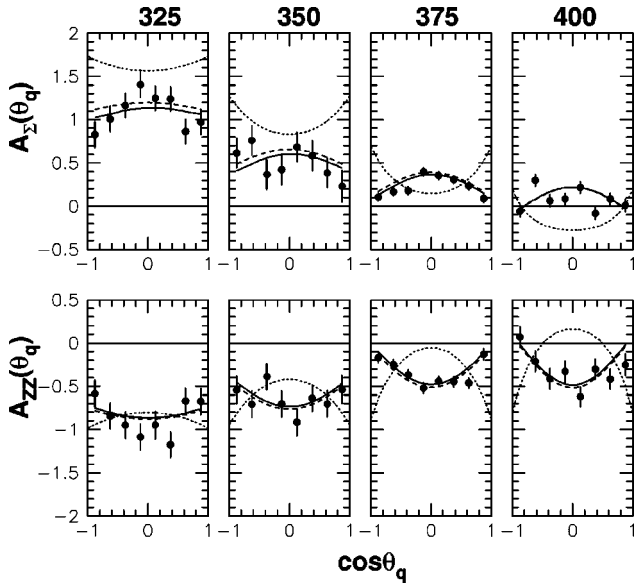

FIG. 5. The observables $A_\Sigma(\theta_q)$ and $A_{zz}(\theta_q)$ as a function of bombarding energy. The dashed curve is obtained with the coefficients of Table IV inserted into Eqs. (11). The solid line is the same but takes into account the real acceptance of the detector (see Sec. IV F). The current status of the theory is illustrated by the dotted line (see Sec. V B).

Some of the 25 observables that are determined in this manner are displayed in Figs. 5–9. Figures 5 and 6 show the spin correlation coefficients $A_\Sigma(\theta)$ and $A_{zz}(\theta)$ as a function of θ_q and θ_p, respectively, for all four bombarding energies. Figure 7 shows the analyzing power $A_{y0}^{\varphi_q}(\theta_q)$ and the two spin correlation coefficients $A_{xz}^{\varphi_q}(\theta_q)$ and $A_\Delta^{\varphi_q}(\theta_q)$ that would be measured if only the pion were observed, i.e., if the direction of the relative pp momentum is ignored. Similarly,

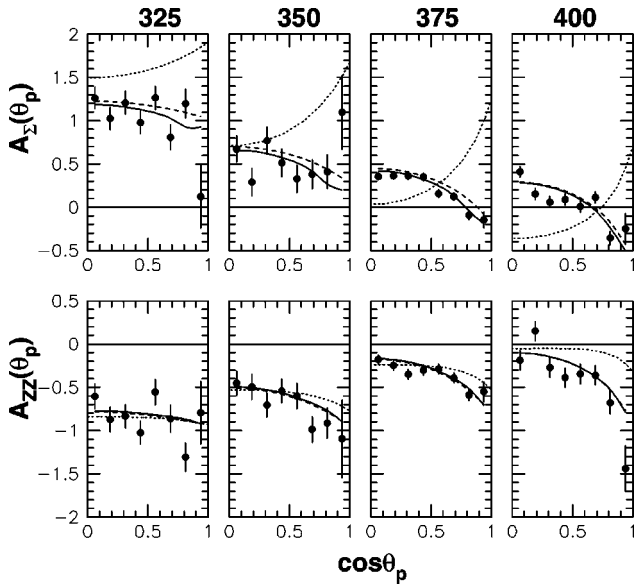

FIG. 6. The observables $A_\Sigma(\theta_p)$ and $A_{zz}(\theta_p)$ as a function of bombarding energy. The curves are explained in the caption of Fig. 5.

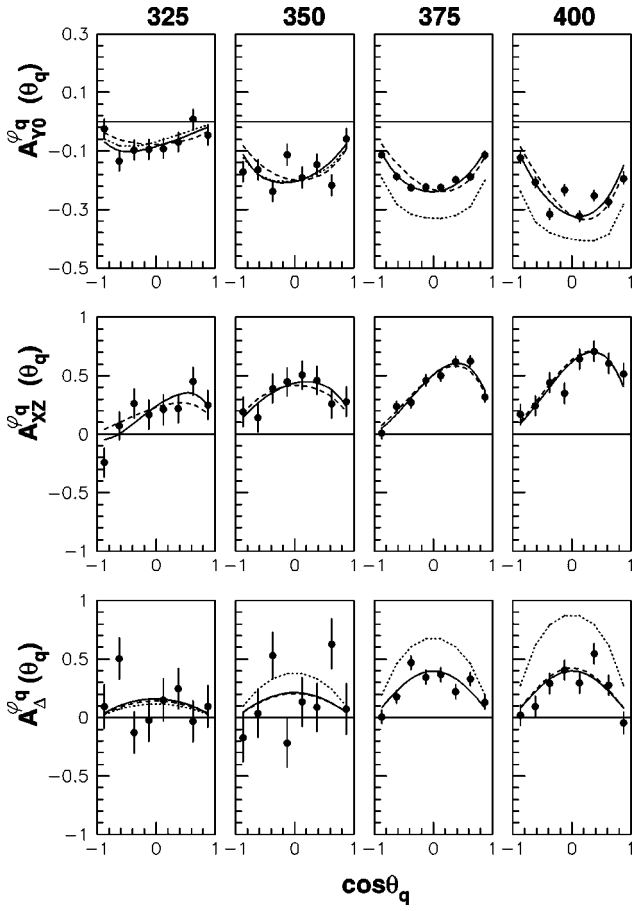

FIG. 7. $A_{y0}^{\varphi_q}(\theta_q)$, $A_{xz}^{\varphi_q}(\theta_q)$, and $A_\Delta^{\varphi_q}(\theta_q)$ at all four bombarding energies. These observables are based on the direction of the π^0; i.e., the relative proton momentum is ignored. The curves are explained in the caption of Fig. 5.

Fig. 8 shows these observables for the case where the pion direction is ignored. In Fig. 9, some of the remaining possible observables are shown at 375 MeV, the energy with the best statistics. The errors shown in these figures are from counting statistics only. The solid curve is obtained from Eq. (11) with the coefficients in Table IV, taking into account the restricted acceptance of the detector system, while the dashed curve results when a detector with 100% acceptance is assumed. The only significant effect of the restricted acceptance occurs with the observables A_Σ and A_{zz}. The dotted curves are theoretical calculations that will be discussed later.

C. A_{z0} and A_Ξ

The longitudinal analyzing power A_{z0} and the combination $A_\Xi \equiv A_{xy} - A_{yx}$ of spin correlation coefficients are proportional to $\sin\Delta\varphi$ or $\sin 2\Delta\varphi$ [Eq. (11)], where $\Delta\varphi \equiv \varphi_p - \varphi_q$. Thus, these observables are invariant with respect to a rotation around the beam axis, and they vanish for $\Delta\varphi = 0$ and π, which is the case when the momenta of the three outgoing particles are coplanar. The vanishing of these observables in the case of a coplanar final state is a consequence of parity conservation. In fact, a measurement of A_{z0}

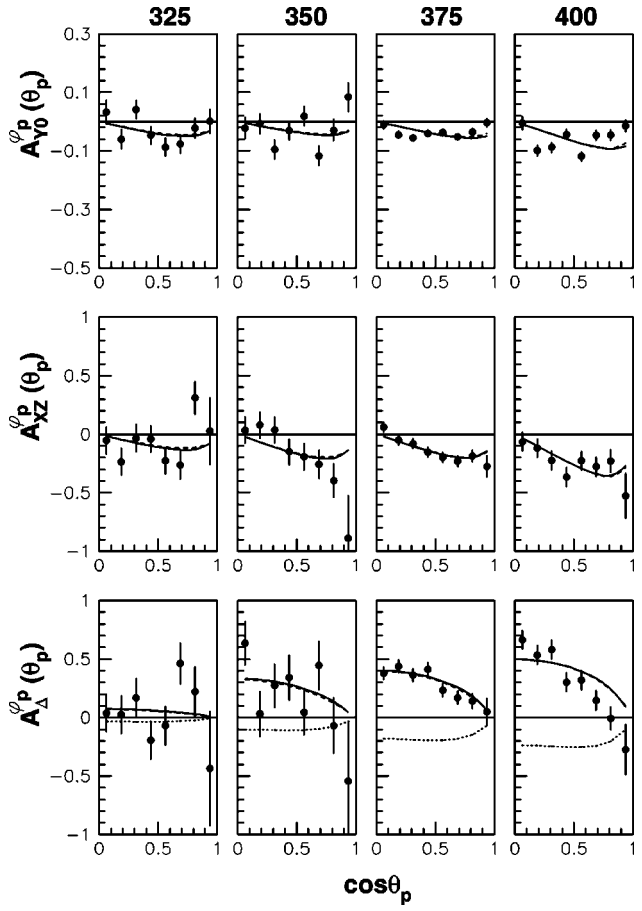

FIG. 8. $A_{y0}^{\varphi_p}(\theta_p)$, $A_{xz}^{\varphi_p}(\theta_p)$, and $A_{\Delta}^{\varphi_p}(\theta_p)$ at all four bombarding energies. These observables are based on the direction of the relative proton momentum; i.e., the π^0 momentum is ignored. The curves are explained in the caption of Fig. 5.

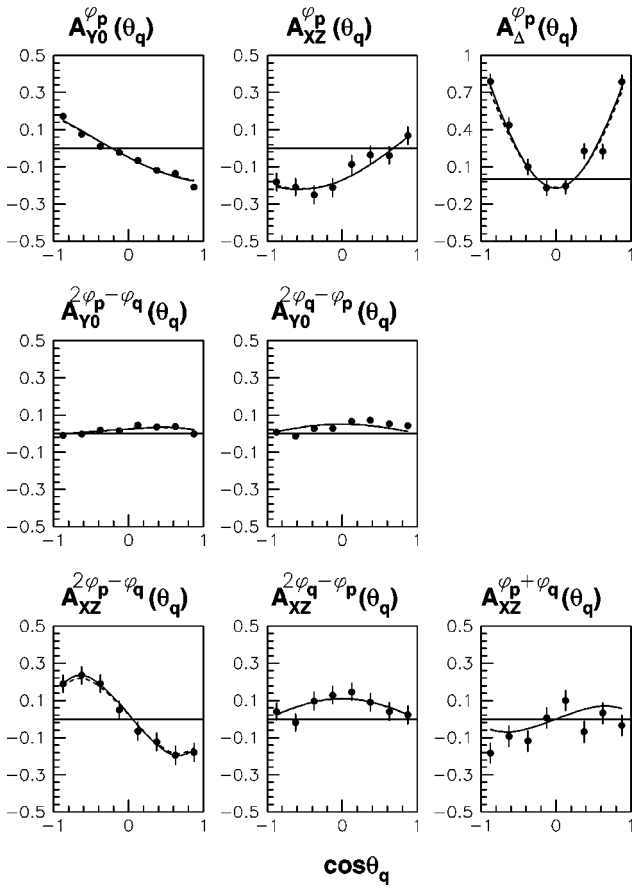

FIG. 9. Some of the observables not shown in Figs. 5–8, at 375 MeV bombarding energy. For these observables the directions of the π^0 *and* of the relative proton momentum have to be known. The curves are explained in the caption of Fig. 5.

in a two-body final-state reaction (thus, in coplanar geometry), or in a total cross section, has been used as a tool to study the violation of parity conservation [16].

Recently, we have published a first analysis [17] of the longitudinal analyzing power A_{z0} for $pp\to pp\pi^0$ in which we demonstrated that this observable can be quite large if noncoplanar final states are involved. Previous measurements of this observable are scarce: some indication of a large value of A_{z0} was found [18] in another pion production reaction, $pn\to pp\pi^-$ at 443 MeV, while a measurement of A_{z0} in the reaction $^2\mathrm{H}(p,pp)n$ at 9 MeV yielded values that are consistent with zero at the level of 0.003 [19].

In analogy with the previous section, we define the observables $A_{z0}^{\Delta\varphi}(\theta_q)$, $A_{z0}^{2\Delta\varphi}(\theta_q)$, and $A_{\Xi}^{\Delta\varphi}(\theta_q)$ as $A_{z0}(\xi)$ and $A_{\Xi}(\xi)$, integrated over θ_p, as well as integrated over azimuth with the condition $\Delta\varphi=$const and evaluated at $\Delta\varphi=\pi/2$. This definition is suggested by Eqs. (11g) and (11h). Again, we can distinguish $A_{z0}^{\Delta\varphi}(\theta_q)$ from $A_{z0}^{2\Delta\varphi}(\theta_q)$ because we know the full $\Delta\varphi$ distribution. Likewise, we define the $\Delta\varphi$ parts of A_{Σ} and A_{zz} as $A_{\Sigma}^{\Delta\varphi}$, $A_{\Sigma}^{2\Delta\varphi}$, $A_{zz}^{\Delta\varphi}$ and $A_{zz}^{2\Delta\varphi}$, in this case evaluated at $\Delta\varphi=0$ [based on Eqs. (11c) and (11d)].

In order to extract A_{z0} and A_{Ξ} from the present data, we generate the asymmetries S_P, S_{Q_j}, and S_{P,Q_j} as a function of $\Delta\varphi$. It is obvious that A_{y0}, A_{xz}, and A_{Δ} do not contribute in this case, since they do not depend on $\Delta\varphi$. Ignoring for the moment a possible $\Delta\varphi$ dependence of the spin-averaged cross section, we obtain, for the asymmetries [analogous to Eqs. (16) and (17)],

$$S_P(\theta,\Delta\varphi)=P_z A_{z0}^{\Delta\varphi}(\theta)\sin 2\Delta\varphi, \tag{18a}$$

$$S_{Q_x}(\theta,\Delta\varphi)=S_{Q_y}(\theta,\Delta\varphi)=0, \tag{18b}$$

$$S_{Q_z}(\theta,\Delta\varphi)=QA_{z0}^{\Delta\varphi}(\pi-\theta)\sin\Delta\varphi+QA_{z0}^{2\Delta\varphi}(\pi-\theta)\sin 2\Delta\varphi, \tag{18c}$$

$$\begin{aligned}S_{P,Q_x}(\theta,\Delta\varphi)=&\,1/2P_xQ[A_{\Sigma}(\theta)+A_{\Sigma}^{\Delta\varphi}(\theta)\cos\Delta\varphi\\&+A_{\Sigma}^{2\Delta\varphi}(\theta)\cos 2\Delta\varphi]\\&-1/2A_{\Xi}^{\Delta\varphi}(\theta)P_yQ\sin\Delta\varphi,\end{aligned} \tag{18d}$$

$$\begin{aligned}S_{P,Q_y}(\theta,\Delta\varphi)=&\,1/2P_yQ[A_{\Sigma}(\theta)+A_{\Sigma}^{\Delta\varphi}(\theta)\cos\Delta\varphi\\&+A_{\Sigma}^{2\Delta\varphi}(\theta)\cos 2\Delta\varphi]\\&+1/2A_{\Xi}^{\Delta\varphi}(\theta)P_xQ\sin\Delta\varphi,\end{aligned} \tag{18e}$$

TABLE IV. Values at the four bombarding energies of the coefficients introduced in Eqs. (11). The derivation of these coefficients is discussed in Sec. IV D. All values have been normalized with the common factor $8\pi^2/\sigma_{tot}$. These numbers parametrize all possible initial-state polarization observables of the reaction everywhere in phase space.

	325 MeV		350 MeV		375 MeV		400 MeV	
	Value	Error	Value	Error	Value	Error	Value	Error
E	0.721	0.082	0.410	0.086	0.221	0.030	0.043	0.053
F^1	0.168	0.021	0.265	0.022	0.262	0.007	0.297	0.013
H_0^{00}	0.111	0.005	0.325	0.010	0.517	0.015	0.660	0.010
H_0^{Σ}	0.056	0.059	0.289	0.060	0.369	0.038	0.603	0.048
H_0^{zz}	0.055	0.082	0.036	0.086	0.148	0.030	0.057	0.053
$H_1^{00}+I$	0.014	0.082	0.041	0.086	0.063	0.030	0.084	0.053
$H_2^{00}+F_2+K$	−0.008	0.416	−0.059	0.419	−0.118	0.402	−0.170	0.406
$H_1^{\Sigma}+2I$	−0.017	0.060	−0.051	0.064	−0.080	0.020	−0.105	0.028
$H_2^{\Sigma}-2F_2+2K$	−0.078	0.080	−0.167	0.094	−0.215	0.024	−0.248	0.114
$H_1^{zz}-I$	0.031	0.056	0.092	0.058	0.143	0.023	0.189	0.045
$H_2^{zz}-F_2-K$	−0.046	0.079	−0.104	0.080	−0.139	0.030	−0.166	0.059
G_1^{z0}	−0.096	0.010	−0.223	0.022	−0.296	0.030	−0.344	0.034
G_1^{Ξ}	−0.158	0.016	−0.365	0.037	−0.486	0.049	−0.564	0.056
H_1^{z0}	0.019	0.002	0.057	0.006	0.089	0.009	0.117	0.012
H_2^{z0}	−0.054	0.052	0.020	0.047	−0.041	0.020	0.000	0.032
H_4^{00}	−0.013	0.006	−0.038	0.018	−0.060	0.029	−0.079	0.038
H_5^{00}	−0.056	0.006	−0.165	0.018	−0.257	0.029	−0.325	0.038
H_4^{Σ}	−0.038	0.019	−0.122	0.055	−0.175	0.086	−0.231	0.114
H_5^{Σ}	−0.133	0.019	−0.389	0.055	−0.607	0.086	−0.688	0.090
H_4^{zz}	0.025	0.019	0.074	0.055	0.115	0.080	0.152	0.114
H_5^{zz}	0.074	0.019	0.217	0.055	0.339	0.080	0.363	0.114
G_1^{y0}	−0.079	0.016	−0.196	0.016	−0.223	0.005	−0.291	0.009
G_2^{y0}	0.009	0.020	−0.023	0.022	0.026	0.007	0.048	0.011
G_3^{y0}	−0.018	0.038	−0.149	0.038	−0.298	0.013	−0.347	0.021
G_4^{y0}	0.018	0.024	0.037	0.024	0.031	0.008	0.030	0.014
G_1^{xz}	0.223	0.058	0.396	0.056	0.473	0.022	0.574	0.040
G_2^{xz}	0.058	0.083	−0.043	0.083	0.024	0.029	0.040	0.054
G_3^{xz}	0.146	0.140	0.017	0.136	0.245	0.051	0.195	0.093
G_4^{xz}	0.045	0.086	−0.031	0.086	0.035	0.032	0.085	0.059
$H_1^{y0}+I^{y0}$	0.030	0.019	0.016	0.019	0.000	0.006	−0.029	0.011
$H_3^{y0}+K^{y0}$	−0.051	0.019	−0.045	0.019	−0.049	0.006	−0.061	0.011
H_4^{y0}	0.006	0.019	−0.019	0.019	0.018	0.006	0.028	0.011
H_5^{y0}	−0.011	0.029	0.039	0.029	0.021	0.010	0.024	0.016
H_6^{y0}	−0.016	0.029	0.121	0.029	0.071	0.010	0.062	0.016
$H_1^{xz}+I^{xz}$	0.064	0.068	0.027	0.068	0.203	0.025	0.216	0.047
$H_3^{xz}+K^{xz}$	−0.123	0.068	−0.193	0.068	−0.188	0.025	−0.316	0.047
H_4^{xz}	−0.101	0.070	−0.086	0.068	0.051	0.028	−0.053	0.049
H_5^{xz}	0.016	0.102	−0.259	0.102	−0.315	0.038	−0.391	0.070
H_6^{xz}	0.027	0.102	0.157	0.102	0.153	0.038	0.208	0.070
H_1^{Δ}	0.135	0.081	0.194	0.099	0.374	0.027	0.379	0.039
H_2^{Δ}	−0.069	0.120	−0.020	0.141	−0.008	0.036	0.072	0.054
H_3^{Δ}	0.071	0.081	0.339	0.099	0.441	0.027	0.567	0.039
H_4^{Δ}	0.137	0.081	0.429	0.102	0.536	0.027	0.567	0.027
H_5^{Δ}	−0.030	0.135	0.093	0.158	0.106	0.045	0.198	0.068

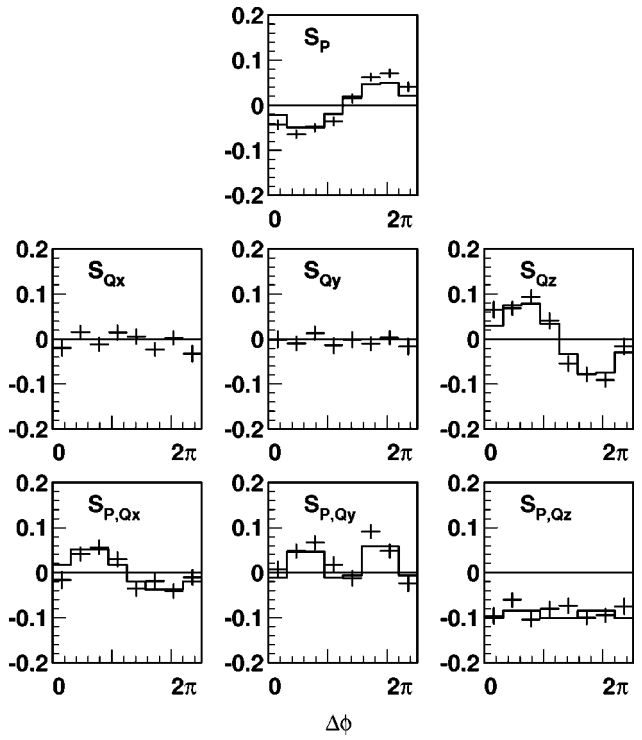

FIG. 10. The asymmetries versus $\Delta\varphi \equiv \varphi_p - \varphi_q$ at 375 MeV bombarding energy. Integrated over both polar angles, the curves represent a fit to the $\Delta\varphi$ distribution according to Eq. (18).

$$S_{P,Q_z}(\theta,\Delta\varphi) = P_z Q[A_{zz}(\theta) + A_{zz}^{\Delta\varphi}(\theta)\cos\Delta\varphi + A_{zz}^{2\Delta\varphi}(\theta)\cos 2\Delta\varphi]. \quad (18f)$$

These asymmetries, integrated over polar angle, are shown in Fig. 10. Here, S_P and S_{Q_z} reflect the beam and target analyzing powers A_{z0} and A_{0z}, which are related by Eq. (7). The quantities S_{Q_x} and S_{Q_y} are consistent with zero, as expected.

Evaluating the asymmetries as a function of θ_q (thus, integrating over θ_p), we extract the θ_q distributions of the observables by fitting with the respective functions of $\Delta\varphi$. In this way we obtain the observables

$$A_{z0}^{\Delta\varphi}(\theta_q), \quad A_{\Xi}^{\Delta\varphi}(\theta_q) \quad (\Delta\varphi = \pi/2), \quad (19)$$

$$A_{\Sigma}^{\Delta\varphi}(\theta_q), \quad A_{zz}^{\Delta\varphi}(\theta_q) \quad (\Delta\varphi = 0),$$

$$A_{\Sigma}^{2\Delta\varphi}(\theta_q), \quad A_{zz}^{2\Delta\varphi}(\theta_q) \quad (\Delta\varphi = 0).$$

The part of A_{z0} that scales with $\sin 2\Delta\varphi$ [see Eq. (11g)] was found to be consistent with zero. It is clear from Eqs. (11g) and (11h) that the θ_p dependence does not contain independent information. Thus, from the $\Delta\varphi$-dependent asymmetries we extract six additional observables. They are shown in Fig. 11 for the measurements with better statistics at 375 and 400 MeV.

D. Parametrization of the data

The expansion into functions of the angles θ_q, φ_q, θ_p, φ_p [Eq. (11)] allows one to calculate all polarization observables at any point in phase space, provided the expansion coefficients E, F, G, . . . are known. These coefficients thus represent a parametrization of all our measurements and constitute the central result of this experiment. The values for the coefficients, normalized by a common factor $8\pi^2/\sigma_{tot}$, are listed in Table IV. Note that the common factor cancels when calculating a polarization observable A_{ij} by dividing the spin-dependent cross section $\sigma_0 A_{ij}$ by the spin-averaged cross section σ_0.

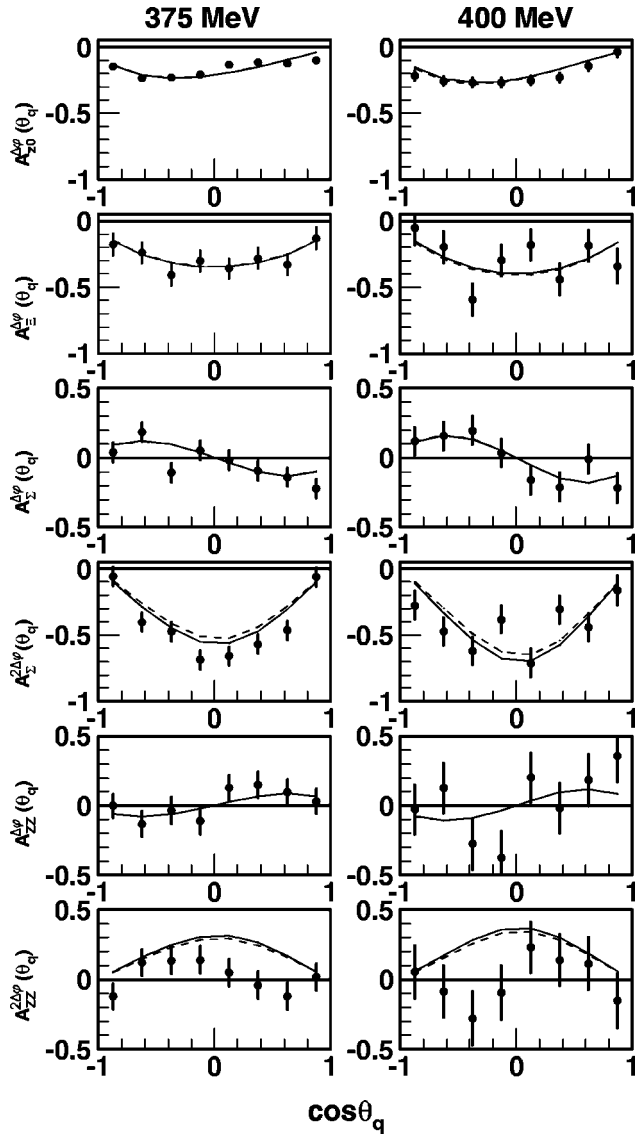

FIG. 11. Polar angle θ_q dependence of the observables that depend on $\Delta\varphi \equiv \varphi_p - \varphi_q$, as discussed in Sec. IV C, at the two bombarding energies with the best statistics. The curves are explained in the caption of Fig. 5.

The task of determining the values of the coefficients of Eqs. (11) is simplified by the fact that a given polarization observable from the list in Eqs. (15) and (19) depends on only a few coefficients. For instance, the observable $A_{y0}^{\varphi_q}(\theta_q)$ depends on G_1^{y0}, $(H_1^{y0} + I^{y0})$, and $(H_1^{00} + I)$, and $A_{y0}^{\varphi_q}(\theta_p)$ depends on G_1^{y0}, G_2^{y0}, and $(H_2^{00} + F_2 + K)$. However, the quality of the data, especially at the lower two energies, is

TABLE V. Total cross sections versus bombarding energy. The second column lists the spin-averaged total cross section assumed in this paper. The next two columns show the result of this experiment for the spin-dependendent total cross sections. These values have been corrected for incomplete detector acceptance by the amount listed in the last two columns (see Sec. IV F).

T (MeV)	$\sigma_{tot}(\eta)$ (μb)	$\Delta\sigma_T/\sigma_{tot}$	$\Delta\sigma_L/\sigma_{tot}$	Corrections $\delta(\Delta\sigma_T/\sigma_{tot})$	$\delta(\Delta\sigma_L/\sigma_{tot})$
325	7.7	-1.162 ± 0.063	1.668 ± 0.116	-0.106	0.026
350	17	-0.579 ± 0.068	1.278 ± 0.114	-0.095	0.026
375	40	-0.287 ± 0.018	0.671 ± 0.046	-0.059	0.021
400	86	-0.096 ± 0.030	0.565 ± 0.088	-0.020	-0.001

not sufficient to fit the coefficients to the data without any constraining assumptions. In the following, we describe these assumptions and a step-by-step procedure to determine the coefficients of Eq. (11).

In the first step, we address the coefficients E, F_1, H_0^{00}, H_0^{Σ}, and H_0^{zz}. The corresponding terms in Eq. (11) do not depend on angle but represent different final states $(\mathbf{Ss})^2$, $(\mathbf{Ps})^2$, and $(\mathbf{Pp})^2$ (see Table II). The relative weight of the $(\mathbf{Ps})^2$ final state follows from the spin-dependent total cross section [Eq. (13)], but the relative contributions of the $(\mathbf{Ss})^2$ and $(\mathbf{Pp})^2$ final states can only be distinguished because they depend on energy ϵ differently. This is explained in more detail in Sec. IV E. Using that result, we set the coefficient H_0^{00} equal to $\sigma(Pp)/\sigma_{tot}$, the relative contribution of the $(\mathbf{Pp})^2$ final state. Having fixed the $(\mathbf{Pp})^2$ strength, the coefficients E, F_1, H_0^{00}, H_0^{Σ}, and H_0^{zz} follow from Eqs. (12), with the values of the spin-dependent total cross sections $\Delta\sigma_T/\sigma_{tot}$ and $\Delta\sigma_L/\sigma_{tot}$, which have been deduced from the total, spin-dependent yields as listed in Table V.

Next, we turn to the coefficients that multiply the terms with $(3\cos^2\theta-1)$ in σ_0, $\sigma_0 A_{\Sigma}$, and $\sigma_0 A_{zz}$ [Eqs. (11a), (11c), (11d)]. Those coefficients are H_1^{00}, H_1^{Σ}, H_1^{zz}, H_2^{00}, H_2^{zz}, and F_2, two of which can be eliminated by Eq. (12d). The **SsSd** and **SsDs** interference terms, I and K may be lumped with the corresponding H_k^{ij} terms with Eq. (12d) still satisfied. Since calculating the observables $\sigma_0 A_{ij}/\sigma_0$ involves a ratio of similar functions, the statistical accuracy of the present data is insufficient to determine these coefficients separately for each bombarding energy. Instead, we impose an energy dependence on the coefficients by setting $H_k^{ij}(\eta) = \overline{H_k^{ij}} \cdot \eta^8/\sigma_{tot}(\eta)$ and $F_2(\eta) = \overline{F_2(\eta)} \cdot \eta^6/\sigma_{tot}(\eta)$. The justification for this assumption is given in the next section, and the values for $\sigma_{tot}(\eta)$ are those listed in Ref. [11] and in Table V. Thus, we fit five variables to the angular distributions $A_{\Sigma}(\theta_q)$, $A_{\Sigma}(\theta_p)$, $A_{zz}(\theta_q)$, and $A_{zz}(\theta_p)$ at all four energies simultaneously. The fit is shown as a solid line in Figs. 5 and 6; the χ^2 per degree of freedom is 1.5.

Next, we determine the coefficients H_k^{00}, H_k^{Σ}, H_k^{zz} $(k=4,5)$, H_1^{z0}, G^{z0}, and G^{Ξ} that appear with terms that contain $\Delta\varphi$. Again, Eq. (12d) constrains the H_k^{ij}. The corresponding observables have been discussed in Sec. IV C. We again impose a bombarding energy dependence of the H coefficients as described in the preceding paragraph and set $G^{ij}(\eta) = \overline{G^{ij}}\,\eta^7/\sigma_{tot}(\eta)$. The remaining seven variables are then fit to the angular distributions $A_{\Sigma}(\theta_q)$, $A_{\Sigma}^{\Delta\varphi}(\theta_q)$, $A_{\Sigma}^{2\Delta\varphi}(\theta_q)$, $A_{zz}(\theta_q)$, $A_{zz}^{\Delta\varphi}(\theta_q)$, $A_{zz}^{2\Delta\varphi}(\theta_q)$, $A_{z0}^{\Delta\varphi}(\theta_q)$, and $A_{\Xi}^{\Delta\varphi}(\theta_q)$ at all four energies simultaneously. The fit is shown as a solid line in Fig. 11; the χ^2 per degree of freedom is 1.6.

With the angular dependence of the spin-averaged cross section now known, the remaining coefficients are determined by fitting the corresponding observables without any constraint on their energy dependence. The errors are obtained by propagating the statistical errors of the measurements.

Note that the observables [Eqs. (15) and (19)] are integrated over either θ_p or θ_q and thus do not constrain the coefficients H_3^{00}, H_3^{Σ}, H_3^{zz}, H_2^{x0}, and H_2^{xz}.

The values of the coefficients in Table IV have been obtained from the data by taking into account the incomplete acceptance of the detector (for more detail, see Sec. IV F). The resulting parametrization of the data is shown as a solid line in Figs. 5–9. Using the same coefficients, but pretending that the detector accepts all of phase space, leads to the dashed line. This illustrates the smallness of the effect of incomplete detector acceptance.

We note that the coefficients I and K that represent interfering **SsSd** and **SsDs** amplitudes always occur in a sum with an H_k^{ij} coefficient. These sums become a single parameter in the analysis. Thus, the present analysis provides no information on the importance of these terms.

Equations (11) contain a total of 49 coefficients. Of these, we determine 44 from the data (see Table IV). Among these, there are six known relations [Eqs. (12a), (12d)], resulting in 38 numbers determined. On the other hand, the coefficients are (known) functions of the amplitudes listed in Table I. Ignoring contributions from **Sd** and **Ds** amplitudes, there are 12 amplitudes. Since there is no interference between amplitudes with $s_f=0$ and $s_f=1$, there are two free phases, and, in principle 22 real numbers should be sufficient to completely describe the data. Thus, the parametrization presented here [Eq. (11) and Table IV] has some redundancy; i.e., there are relations between the parameters [in addition to those in Eq. (12)]. These relations will be revealed in the course of the amplitude analysis which is planned for the future.

E. Energy dependence

1. Definitions and kinematics relation

A complete description of the final-state kinematics, apart from the four angles θ_p, φ_p, θ_q, φ_q, must include an en-

ergy variable that specifies the sharing of the available kinetic energy between the pion and the NN pair. There is only one such variable since the total energy of the system, $\sqrt{s}$, is determined by the bombarding energy. For instance, if q is the magnitude of the pion center-of-mass momentum, the proton momentum in the NN rest system is given by

$$p=\frac{1}{2}\sqrt{s_{12}-4m_p^2}\approx q_{\max}\sqrt{1-(q/q_{\max})^2}, \tag{20}$$

where $s_{12}=s-2\sqrt{s(q^2+m_\pi^2)}+m_\pi^2$ is the square of the energy of the NN subsystem. The second part of Eq. (20) is the corresponding nonrelativistic expression, which is a good approximation near threshold. Here, $q_{\max}$ [Eq. (1)] is the largest possible pion momentum, which is realized when the two protons are at rest relative to each other ($p=0$). In the following, we use as the energy-sharing variable, the kinetic energy ϵ in the NN subsystem given by

$$\epsilon=\sqrt{s_{12}}-2m_p, \tag{21}$$

which ranges from $\epsilon=0$ (when $q=q_{\max}$) to $\epsilon_{\max}=\sqrt{s}-2m_p-m_\pi$ (when $q=0$). The value for $\epsilon_{\max}$ is determined by the bombarding energy, or η [Eq. (2)], as listed in Table III for the energies of this experiment. Using Eqs. (20) and (21), p and q may be expressed in terms of ϵ.

2. Leading contributions to the energy dependence

For a limited energy range, the *dynamics* of pion production is often considered energy independent. The strong energy dependence of the *observables* near threshold is then due to a number of known factors, as discussed in the following.

The first energy dependence is due to the phase space volume $d\rho(\epsilon)$. Nonrelativistically the phase space volume is proportional to $q(\epsilon)p(\epsilon)d\epsilon$. The second energy-dependent factor arises from the radial wave functions for the pion and the NN pair. Close to threshold, the momenta q and p, and thus the arguments of these wave functions, are small, and one can use their limiting form to obtain the factor $q^{l_q}p^{l_p}$, where l_q and l_p are the respective angular momenta. It is this factor that makes it possible to use the energy dependence of the reaction to make statements about partial-wave contributions, but one must keep in mind that the simple power law is an approximation, strictly true only for $p\to 0$ or $q\to 0$.

The third energy-dependent factor arises from distortion in the entrance and exit channel. By far the strongest energy dependence is due to the final-state interaction (FSI) between two nucleons in a relative S state. Watson showed [20] that the FSI energy dependence of the cross section can be separated as a factor $f(\epsilon)$ that follows from the NN phase shifts at energy ϵ. One method to calculate $f(\epsilon)$ is by representing the S-wave phase shift by an effective-range expansion. Since the two nucleons carry charge, Coulomb repulsion has to be incorporated into the effective-range expansion [21]. In the present work, this procedure is adopted for calculations that involve FSIs. Other authors have used a fit to a phenomenological representation of the NN interaction to obtain $f(\epsilon)$ [10].

When integrating over the energy-sharing parameter ϵ one obtains, via the upper limit $\epsilon_{\max}$, a dependence on bombarding energy, or η. Thus, close to threshold, where only the **Ss** wave contributes, the shape of total $pp\to pp\pi^0$ cross section as a function of bombarding energy should be determined by the phase space and FSI, an expectation that is borne out by the data [5]. However, in order to reproduce the measured proton angular distributions, one has to use a value -1.5fm for the scattering length (see Ref. [5]). This is significantly larger than the accepted, Coulomb-uncorrected value for the pp scattering length of $a_{pp}=-7.82\pm 0.01$fm [22]. This indicates clearly that factorizing the FSI of the protons and neglecting all other distortions in the initial and final states is only an approximation (for more on this topic, see Ref. [23]).

In Eq. (11), the partial-wave coefficients E, F_k, G_k^{ij}, H_k^{ij}, I, and K may be integrated over ϵ. This integration is independent of the angular variables since ϵ ranges from 0 to $\epsilon_{\max}$ for any choice of angles.

To reveal the explicit energy dependence of these coefficients, we separate off the probability $w_L(\epsilon)$ with which a given ϵ occurs where L denotes the set of four final-state angular momenta, l_p, l_q, l_p', and l_q', that occur in the bilinear sums of amplitudes,

$$w_L(\epsilon)d\epsilon=\zeta\ \ q(\epsilon)^{1+l_q+l_q'}\,p(\epsilon)^{1+l_p+l_p'}\,f_L(\epsilon)\ \ d\epsilon, \tag{22}$$

where the normalization ζ ensures that $\int w_L(\epsilon)d\epsilon=1$. The final-state factor is given by $f_L(\epsilon)=f(\epsilon)$ if both l_p and l_p' are zero, by $f_L(\epsilon)=\sqrt{f(\epsilon)}$ if either l_p or l_p' is zero, and by $f_L(\epsilon)=1$ in all other cases. The ϵ dependence for partial waves with various angular momenta is given in Table II. The three functions $w_E(\epsilon)$, $w_F(\epsilon)$, and $w_H(\epsilon)$ represent $(\mathbf{Ss})^2$, $(\mathbf{Ps})^2$, and $(\mathbf{Pp})^2$ partial waves. For a bombarding energy of 375 MeV, these three functions are displayed as solid curves in Fig. 12. Note that $w_E(\epsilon)$ clearly shows an enhancement for small ϵ, caused by the final-state interaction. In general, the weight functions $w_L(\epsilon)$ depend on the detector acceptance, since in the laboratory the momenta of the two protons do depend on ϵ. This is illustrated in Fig. 12 by Monte Carlo–generated histograms that show the effect of a 5° central hole in the detector coverage. The consequences of incomplete detector acceptance are discussed further in Sec. IV F.

As briefly noted, the dependence of the amplitudes on ϵ implies a dependence on bombarding energy, or η, because the upper limit $\epsilon_{\max}$ of the integration over ϵ depends on η. In the absence of FSIs, and with the nonrelativistic expression for the phase volume and for $p(\epsilon)$ [Eq. (20)], the integration of Eq. (22) is analytic and a simple power law results. From this, we expect the partial-wave coefficients F, G, and H to be proportional to $\eta^6/\sigma_{tot}(\eta)$, $\eta^7/\sigma_{tot}(\eta)$, and $\eta^8/\sigma_{tot}(\eta)$, respectively. Such a simple dependence on bombarding energy is not expected for the coefficients E, I, and K, since these are affected by the FSI.

3. Dependence of A_Σ and A_{zz} on the energy-sharing parameter

Some of the coefficients in Eq. (11) cannot be distinguished from each other based on the angular distributions.

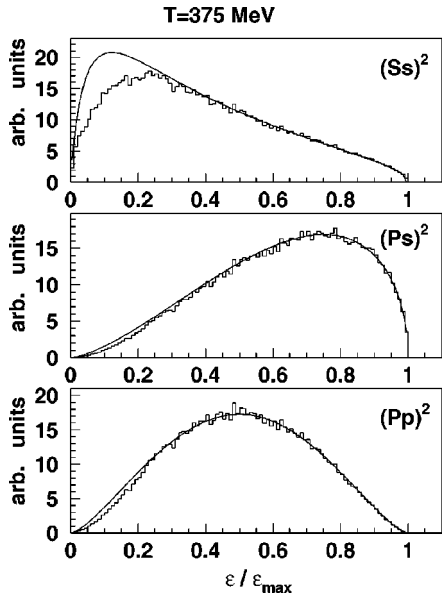

FIG. 12. The probability $w_L(\epsilon)$ as a function of the energy-sharing parameter $\epsilon/\epsilon_{\max}$. The solid line corresponds to Eq. (22), while the Monte Carlo–generated histograms show the effect of the central hole in the detector stack.

However, their individual values can still be assessed, using the fact that they depend differently on the energy parameter ϵ. In this section, we explain how this can be done.

When we integrate the spin-dependent cross sections of Eq. (11) over all angles, only $\sigma_0(\epsilon)$, $\sigma_0(\epsilon)A_\Sigma(\epsilon)$, and $\sigma_0(\epsilon)A_{zz}(\epsilon)$ remain which in turn depend on four coefficients E, F_1, H_0^{00}, H_0^Σ, and H_0^{zz}, where $H_0^{zz}=H_0^{00}-H_0^\Sigma$. Note that these coefficients when normalized by $8\pi^2/\sigma_{tot}$ are related to the partial-wave total cross sections $\sigma(l_p,l_q)$ by $\sigma(Ss)/\sigma_{tot}=E$, $\sigma(Ps)/\sigma_{tot}=F_1$, and $\sigma(Pp)/\sigma_{tot}=H_0^{00}$. The present notation is related to that used in Ref. [11] by $2\hat{\sigma}(Pp)/\sigma_{tot}=H_0^\Sigma$. The two observables $A_\Sigma(\epsilon)$ and $A_{zz}(\epsilon)$ in terms of the partial-wave coefficients are now given by

$$A_\Sigma(\epsilon)=\frac{2[E\cdot w_E(\epsilon)-F_1\cdot w_F(\epsilon)]+H_0^\Sigma\cdot w_H(\epsilon)}{E\cdot w_E(\epsilon)+F_1\cdot w_F(\epsilon)+H_0^\Sigma\cdot w_H(\epsilon)}, \tag{23a}$$

$$A_{zz}(\epsilon)=\frac{-E\cdot w_E(\epsilon)-F_1\cdot w_F(\epsilon)+(H_0^{00}-H_0^\Sigma)\cdot w_H(\epsilon)}{E\cdot w_E(\epsilon)+F_1\cdot w_F(\epsilon)+H_0^\Sigma\cdot w_H(\epsilon)}. \tag{23b}$$

In these equations, the probabilities w_E, w_F, and w_H are known functions of ϵ that differ from each other (see Fig. 12). Thus, it is possible to determine the coefficients E, F_1, H_0^{00}, and H_0^Σ from a fit to the measured $A_\Sigma(\epsilon)$ and $A_{zz}(\epsilon)$. These coefficients are not accessible separately by a study of the angular distributions. A similar method has been applied previously [10] to the spin-averaged total cross section as a function of ϵ.

From the set of good events we determine $A_\Sigma(\epsilon)$ and $A_{zz}(\epsilon)$ following the same procedure as described in Sec. IV B, except that the argument θ_q (or θ_p) is replaced by the energy-sharing parameter ϵ. The result is shown in Fig. 13 for all four bombarding energies. The solid curves are obtained from Eq. (23) with weight functions w_L that take into account the acceptance of the detector. The coefficients in Eq. (23) were forced to depend on bombarding energy as $F_1(\eta)=\tilde{F}_1\eta^6/\sigma_{tot}(\eta)$, $H_0^{00}(\eta)=\tilde{H}_0^{00}\eta^8/\sigma_{tot}(\eta)$, and $H_0^\Sigma(\eta)=\tilde{H}_0^\Sigma\eta^8/\sigma_{tot}(\eta)$. At $T=325$ MeV an accurate value for the total cross section exists ($\sigma_{tot}=7.70\pm0.26\,\mu$b [5]). However, at higher energies, data are few and of poor quality. For the present purpose we use for $\sigma_{tot}(\eta)$ a smooth approximation to the world's data (see Ref. [11] and Table V) Assuming that there are no other partial waves, we have $E=1-F_1-H_0^{00}$. Therefore, only three energy-independent parameters are adjusted. The χ^2 of the best fit per degree of freedom is 1.8, which leads us to suspect that the limitations of the simple energy dependence adopted here may be noticeable, especially at the higher energies. The resulting partial-wave contributions to the total cross section are shown in Fig. 14. The error bars are obtained by repeating the fit by varying the values assumed for σ_{tot} or by using

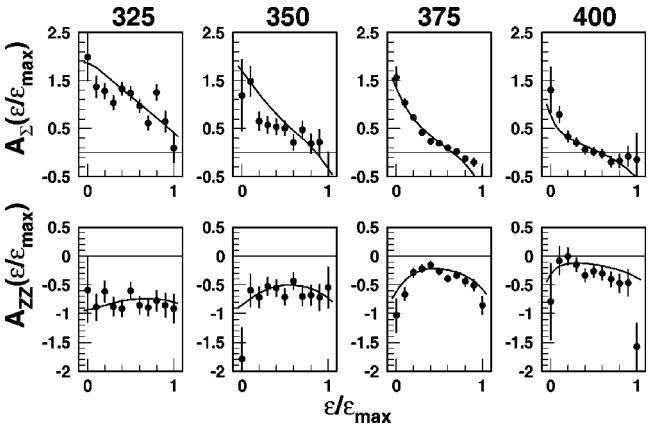

FIG. 13. Dependence of A_Σ and A_{zz}, integrated over both polar angles, on the energy-sharing parameter $\epsilon/\epsilon_{\max}$. The solid lines represent a three-parameter fit to the data at all four energies simultaneously; see Sec. IV E 3.

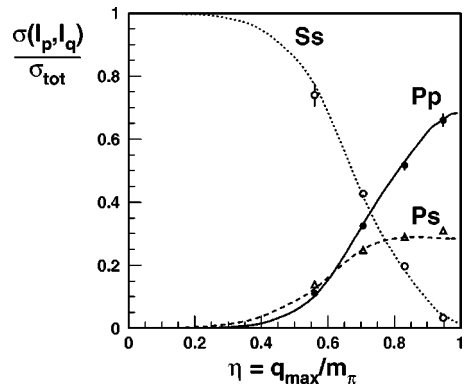

FIG. 14. Contribution of the three possible final-state angular momenta to the total cross section. The dashed and solid lines represent the expected η^6 (η^8) dependence of the **Ps** (**Pp**) partial-wave cross section, while the dotted line indicates the remainder, which represents the **Ss** partial-wave cross section.

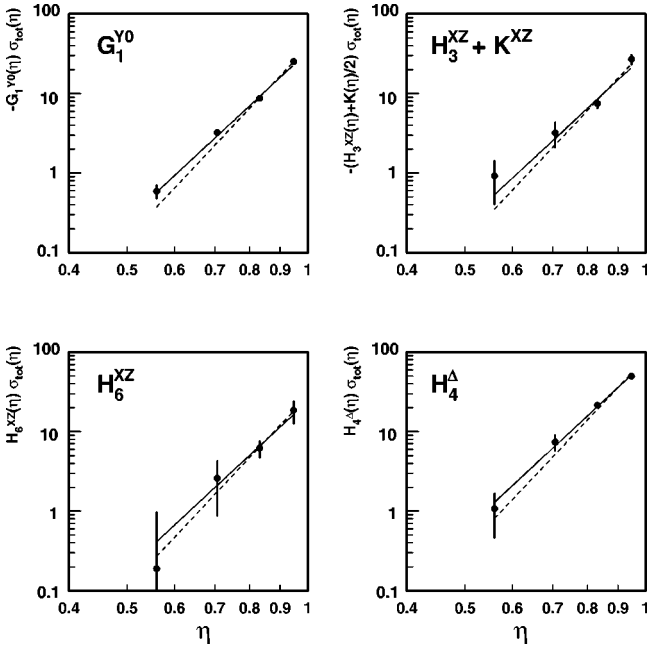

FIG. 15. Dependence of some of the coefficients of Eqs. (11) and Table IV on the bombarding energy. The two lines are proportional to η^7 (solid) (expected for the G coefficients) and η^8 (dashed) (expected for the H coefficients).

weight functions w_L calculated directly from Eq. (22), as would be appropriate for a detector with 100% acceptance. The dashed line in Fig. 14 represents the expected η^6 dependence of the **Ps** partial cross section, $\sigma(\mathbf{Ps})=F_1$, and the solid line corresponds to the imposed η^8 dependence of $\sigma(\mathbf{Pp})=H_0^{00}$, while the dotted line indicates the remainder, given by $E=1-F_1-H_0^{00}$, which represents the **Ss** partial-wave cross section.

4. Dependence of observables on bombarding energy

As pointed out at the end of Sec. IV E 1, based on the phase space, angular momentum dependence of the wave functions, and FSI, we expect that the partial-wave coefficients F, G, and H times the total cross section $\sigma_{tot}(\eta)$ are proportional to η^6, η^7, and η^8, respectively. We have also explained that the integration over ϵ is independent of the angular variables. Thus, each of the coefficients in Eq. (11) that does not contain a NN S state (F, G, and H coefficients) is expected to obey such a power law. In order to test this expectation, we have to multiply the values for the coefficients in Table IV by the total cross section $\sigma_{tot}(\eta)$ at the corresponding energy. For $\sigma_{tot}(\eta)$ we use a smooth approximation to the world's data, as explained in the previous section. The resulting η dependence of some of the coefficients in Table IV that have been obtained without constraining their energy dependence is shown in Fig. 15. The two lines shown in the figure correspond to the best fit with an η^7 or η^8 dependence. As can be seen, the simple power-law η dependence of the coefficients is at least qualitatively correct. This is also true for the coefficient $(H_3^{xz}+K/2)$, which could in principle contain a contribution from a **Ds** amplitude. The observation that the G and H coefficients obey the power law that is expected from the ''trivial'' energy-dependent factors confirms a similar finding based on partial-wave contributions to the spin-dependent total cross sections [11].

F. Systematic uncertainties and corrections

1. Corrections for a nonideal detector

For a number of reasons, the apparatus does not registers all the generated $pp\rightarrow pp\pi^0$ events. The main loss of events occurs because the detector system has a hole in the center to allow for the 3-cm-diam beam pipe just downstream of the target. Seen from the center of the target, this hole subtends a cone with about 5° opening angle. Between 25% (at 325 MeV) and 10% (at 400 MeV) of all events have at least one proton that falls into this cone. At 400 MeV a few percent of the events miss the detector on the outside, and about 3% contain a proton that is energetic enough to fire the veto detector. In about 2% of the events, both protons strike the same segment of the E detector, and therefore do not trigger the detector. The efficiency of an individual wire chamber plane is between 93% and 95%, but since only three planes have to respond for a valid event, only about 8% of all events are lost because of this. All of these effects combined amount to a loss of events between 30% and 22% for the energies from 325 MeV to 400 MeV. A Monte Carlo simulation of the detailed detector performance was used to determine these numbers. Reactions in the scintillators might lower the proton energy measured by the K and E scintillators, leading to a tail of the π^0 peak in the missing-mass spectrum (Fig. 4), placing some good events outside the accepted mass range. However, there is no evidence for a significant tail in the mass spectrum.

The correction of the data presented in this paper for the losses discussed above turns out to be small. This is because polarization observables are a ratio of yields measured with and without polarization. If the fraction of lost events is the same in both cases, there is no net correction. For this reason, there is no correction for the data in a given volume element $d\Omega_p d\Omega_q d\epsilon$ of the five-dimensional phase space. Thus, corrections arise only when integrating over some region of the phase space.

Acceptance corrections are estimated as follows. Let us denote by $\alpha(\xi)$ the detector acceptance at a given point ξ in phase space. Since the corresponding event is either seen or not seen, $\alpha(\xi)$ has a value of 1 or 0. In five-dimensional phase space the transition from $\alpha=0$ to $\alpha=1$ occurs at well-defined boundaries. However, when one integrates over several variables, the dependence of α on the remaining variables is smoothed out, and this is another reason for the smallness of the acceptance corrections. Since the functional dependence of the observables on all five variables θ_q, φ_q, θ_p, φ_p, and ϵ is known, we can carry out the integration over kinematic variables, weighting the integrand with $\alpha(\xi)$ and thus taking into account the real detector acceptance. These integrals are evaluated numerically using the Monte Carlo method for each of the partial waves in Table II and for each of the trigonometric functions of the kinematic vari-

ables. For comparison, setting $\alpha=1$, independent of ξ, yields the result for a detector with 100% acceptance. The effect of incomplete acceptance on the angular distributions is illustrated in Figs. 5–9. The solid curve is obtained from Eqs. (11) and the coefficients in Table IV using the true detector acceptance, while the dashed line results when 100% detector acceptance is assumed. As can be seen the effects are very small.

The acceptance corrections for the total cross sections, Eq. (12), involve the integrals over the entire phase space for three partial waves with the final states **Ss**, **Ps** and **Pp**, corresponding to E, F_1, and H in Eq. (12). Again, if the fractional loss for all three partial waves were the same, there would be no correction. However, as can be seen from Fig. 12, the **Ss** partial wave is affected more strongly by losses in the central hole than the other two partial waves. In order to evaluate the correction for $\Delta\sigma_T/\sigma_{tot}$ and $\Delta\sigma_L/\sigma_{tot}$ the relative strength of the three partial waves is taken as shown in Fig. 14. The resulting corrections are listed in Table V. They are slightly different than those used in Ref. [11] because more has since been learned about the relative importance of the three contributing partial waves.

2. Other systematic effects

The dead time of the data acquisition system was measured for each of the different spin states of beam and target. The dead time is a few percent and differences between spin states are less than 10^{-3}. Thus, dead time effects can be neglected.

The reconstruction of the pion polar angle θ_q depends sensitively on the absolute energy calibration of the E and K scintillators, since the pion has to account for the remaining momentum. However, because of the identity of the collision partners, the spin-averaged cross section has to be symmetric around $\theta_q=90°$. This condition has been used as one of the criteria in determining the energy calibration of the scintillators.

Finally, one has to worry about the resolution of the detector system as a whole for the cms angles $\theta_p, \phi_p, \theta_q$, and ϕ_q. This has been studied with a Monte Carlo simulation of the response of the detector system. The generated events were processed by the same code that was used to analyze the data. For all four angles, the difference between the reconstructed angle and the ''true'' angle (as chosen initially by the Monte Carlo simulation) falls into a distribution which is very nearly a Gaussian, centered on zero within the widths of the distributions. We identify the angular resolution with the σ of this Gaussian in each case. These distributions vary somewhat with beam energy and are widest for the lowest-energy data. Therefore, we here report the σ of the Gaussian fit to each distribution at 325 MeV beam energy. The results are $\sigma=3.0°$ for θ_p, 1.5° for ϕ_p, 8.0° for θ_q, and 6.0° for ϕ_q. The σ corresponding to the $\cos(\theta_p)$ distribution of errors is 0.04, and for $\cos(\theta_q)$ it is 0.12. There is no correlation observed between the errors in the reconstructed p and q vectors. Clearly, this resolution is sufficient to resolve the harmonic content of the angular distributions in this experiment.

V. COMPARISON WITH THEORY

A. Current status of the theory of $NN\rightarrow NN\pi$

The advent of new data due to the three technical advances mentioned in Sec. I was answered by theoretical developments. The first measurements triggered a study of quantum number selection rules, of the role of the final-state interaction, and of nucleon excited states, and led to a theory of pion production in analogy with quantum electrodynamics. The availability of kinematically complete cross section data led to the application of effective chiral Lagrangians, of soft pion techniques, and models with coupled channels, and the recent precise cross section data close to threshold obtained at storage rings stimulated the construction of meson exchange models, and a study of the short-range part of the NN interaction as well as the role of chiral symmetry in the interpretation of pion production. A review of the developement of the theory of πNN systems, prior to 1990 is given in Ref. [24].

We now recognize the fact that the reaction $pp\rightarrow pp\pi^0$ near threshold is sensitive to short-range exchange mechanisms in the two-nucleon system, because the main pion exchange term is prohibited by isospin conservation. Soon after the first accurate total cross section measurement with an electron-cooled beam [5], it was realized [25,26] that pion production on a single nucleon underestimates the empirical cross section by about a factor of 5. Lee and Riska proposed [27] that this shortfall of the theoretical cross section might be explained by the omission of pair diagrams with an exchanged heavy meson (σ, ω). This was confirmed quantitatively [28]. Subsequently, the role of residual, virtual pion exchange was found to be not necessarily small [29,30]. However, at this time the role of pion rescattering is still controversial, especially since field theoretical models and chiral perturbation theory [31,32] disagree on the sign of the pion exchange amplitude. On the other hand, the importance of heavy-meson exchange also has been questioned [33]. Additional short-range mechanisms have been studied as well, including transition couplings between different exchanged mesons [34] and the role of the $\Delta(1232)$ isobar [26,32,30] and the S_{11} and D_{13} nucleon resonances [35]. An interpretation of the reaction on the basis of approximately conserved chiral symmetry [36,37,31,32] has, so far, not been able to reproduce the cross section close to threshold. Fully relativistic calculations have been carried out in a covariant one-boson exchange model with parameters fitted to the amplitudes of elastic NN scattering [38,39].

B. Theory and polarization observables

The impressive theoretical effort during the past decade that is summarized in the preceding section has been mostly devoted to a study of the lowest partial wave. Since, as we have seen, the energy dependence of that partial wave is well described by ''trivial'' factors, this means that, so far, only its strength, i.e., a single experimental number, has been confronted with theory. Some of the models mentioned in the preceding section naturally include higher partial waves and thus would be able to predict polarization observables. How-

ever, at this time, such calculations have only been carried out by groups at Osaka [40] and at Jülich [30,41,42].

Pion production in the Jülich model [43] includes direct production, *s*- and *p*-wave pion rescattering, an intermediate $\Delta(1232)$ nucleon excited state, and a contribution from pair diagrams. The latter carries an adjustable parameter; it is taken to represent those short-range mechanisms that are not explicitly included in the model. Final-state angular momenta up to 2 are included. The prediction of the Jülich model for some of the observables presented in this paper is shown as a dotted line in Figs. 5–8. It is fair to say that there is little similarity between theoretical estimates and the data. We hope that the theoretical community views this disagreement as a challenge.

Finally, we point out that the experimental information now available offers the possibility to discuss individual reaction amplitudes, and that a comparison with theory should take place on this level. Such a study is currently in progress.

VI. SUMMARY AND CONCLUSIONS

We have studied the reaction $pp \rightarrow pp\pi^0$, kinematically complete, with a polarized beam and a polarized target. The experiment relies on the advantages offered by the use of an internal target in a storage ring. The experiment has been carried out at four bombarding energies between 325 and 400 MeV. In this energy range the **Ss** partial wave ceases to be dominant, and higher partial waves become important (see Fig. 14).

Throughout the present energy region, the number of significant partial amplitudes is still small (at most 12). Under these conditions, it is feasible to expand the observables into a complete set of angular functions. The expansion coefficients are determined from the data. This results in a parametrization of the findings of this experiment and allows one to calculate any analyzing power or correlation coefficient for any configuration of the three-body final state. We include as an appendix the necessary framework to discuss polarization observables in a reaction with polarized spin-1/2 collision partners and a three-body final state.

From a formal partial-wave analysis we learn that the amplitudes can be arranged into the two groups (**Ss**, **Sd**, **Ds**) and (**Ps**, **Pp**), and only amplitudes within one group can interfere with each other. We also see that in the coefficients of the angular distributions, terms that represent the interference between (**SsSd**) and (**SsDs**) amplitudes, always occur in a sum with a term that contains only **Pp** waves. These sums then become a single parameter in the analysis. Thus the contribution from **Sd** and **Ds** partial waves cannot be deduced from the angular distribution and must rely on a study of the energy dependence. However, we find no evidence that terms that contain **Sd** and **Ds** partial waves depart in their energy dependence from what is expected for the competing **Pp** wave alone.

The formalism presented in this paper shows that it is possible to calculate the observables from the partial-wave amplitudes directly. Embedding this calculation into a fitting procedure would allow one to discuss the constraints on individual amplitudes that follow from the present measurement. Such an amplitude analysis is currently in progress.

ACKNOWLEDGMENTS

This work has been supported by the U.S. National Science Foundation under Grant Nos. PHY-9602872, PHY-9722554, PHY-9722556, and PHY-9901529, and by the U.S. Department of Energy under Grant No. DOE-FG02-88ER40438. We would like to thank Dr. Ch. Hanhart for making available the Jülich-model calculations of some of the observables presented here. We also would like to thank our colleagues M. Dzemidzic, F. Sperisen, M. Wolanski, and R. Flammang who participated in the early phases of this experiment.

APPENDIX: PARTIAL-WAVE FORMALISM

1. Expansion of the reaction amplitude

We present here the details of the partial-wave formalism which was employed to determine the form of the angular distributions of the cross section and polarization observables, Eqs. (11). The main difficulty for reactions such as $pp \rightarrow pp\pi^0$ is to understand how a partial-wave expansion can be carried out for situations in which the final state has three particles.

We work in the c.m. frame and adopt coordinates $\mathbf{r}$ and $\boldsymbol{\rho}$ conjugate to the momenta $\mathbf{p}$ and $\mathbf{q}$ of Fig. 2. The symbol Ψ represents the full wave function of the system that evolves from the pp initial state, and we wish to focus on the components of Ψ which correspond to some three-body channel β. We know from Ref. [44] that for reactions leading to three-body final states, the outgoing wave in the asymptotic region is of the form

$$\Psi_\beta(\boldsymbol{r},\rho) \rightarrow \frac{e^{i\xi R_\beta}}{R_\beta^{5/2}} f_\beta(\boldsymbol{p},q;k_i), \tag{A1}$$

where $\boldsymbol{k}_i$ is the initial momentum. The quantities ξ and R_β are given by

$$\xi^2 = 2\sqrt{\mu_1\mu_2}E_\beta/\hbar^2 \tag{A2}$$

and

$$R_\beta^2 = (\mu_1 r^2 + \mu_2\rho^2)/\sqrt{\mu_1\mu_2}, \tag{A3}$$

where μ_1 and μ_2 are the reduced masses associated with the coordinates $\boldsymbol{r}$ and $\boldsymbol{\rho}$, and E_β is the available kinetic energy in the final state.

If the particles have spin, we may construct a wave function with spin projections σ_a and σ_b for the two particles in the initial state, and the full wave function Ψ that evolves from this initial state will contain outgoing waves with various final-state spin projections σ_1, σ_2, and σ_3. It follows that the reaction amplitudes f_β must carry all five spin labels. Isospin projection quantum numbers may be incorporated in a similar way.

Formal expressions for the reaction amplitudes can be obtained by employing a three-body Green's function [45] in conjunction with a Lippmann-Schwinger-like equation (see Ref. [44]). The result for the asymptotic wave function in channel β is

$$\Psi_\beta(\boldsymbol{r},\boldsymbol{\rho}) \rightarrow i\left(\frac{2}{\pi\xi}\right)^{1/2} \frac{e^{i\xi R_\beta}}{R_\beta^{5/2}} \frac{E_\beta \mu_1 \mu_2}{(2\pi\hbar^2)^2} \langle \psi_f | V_\beta | \Psi \rangle, \quad \text{(A4)}$$

where V_β is some kind of interaction potential and

$$\psi_f = e^{i\boldsymbol{k}\cdot\boldsymbol{r}} e^{i\boldsymbol{q}\cdot\boldsymbol{\rho}} \phi_1 \phi_2 \phi_3 . \quad \text{(A5)}$$

In this last formula the ϕ_i's are the internal wave functions of the particles in the final state. For $pp \rightarrow pp\pi^0$ these are just spin and isospin wave functions. The matrix element in Eq. (A4) implies integration over all coordinates of the problem, and the actual dependence of Ψ_β on $\boldsymbol{r}$ and $\boldsymbol{\rho}$ is contained in the $e^{i\xi R}/R^{5/2}$ factor. The formula for the reaction amplitude can simply be read off from Eq. (A4) with the help of Eq. (A1).

To obtain a partial-wave expansion of f_β we need to expand both Ψ and the outgoing plane waves in terms of angular momentum eigenfunctions. One begins by dividing Ψ into two parts,

$$\Psi = \psi_i + \Phi, \quad \text{(A6)}$$

where ψ_i is the unscattered incident plane wave and Φ is everything else. For ψ_i we write

$$\psi_i = \chi_a^{\sigma_a} \chi_b^{\sigma_b} \eta_a^{\tau_a} \eta_b^{\tau_b} e^{i\boldsymbol{k}_i\cdot\boldsymbol{r}_i}, \quad \text{(A7)}$$

where the χ's and η's are spin and isospin wave functions, respectively.

For the angular momentum expansion we choose basis states that are simultaneous eigenfunctions of the initial total spin s_i, orbital angular momentum l, total angular momentum J, and total isospin t, with the coupling orders $[(s_a,s_b)s_i,l\,]J$ and $(t_a,t_b)t$. We use the symbol ν to denote initial state quantum numbers J, l, s_i, and t. Then, by employing standard angular momentum identities (see, for example, Ref. [46]) we obtain

$$\psi_i = 4\pi \sum_\nu \sum_{M,\lambda,\sigma_i,\tau} \langle s_a\sigma_a, s_b\sigma_b | s_i\sigma_i\rangle \langle s_i\sigma_i, l\lambda | JM\rangle \times \langle t_a\tau_a, t_b\tau_b | t\tau\rangle\, j_l(k_i r_i)\, \mathcal{Y}_\nu^{M,\tau} Y_l^{\lambda *}(\hat{k}_i), \quad \text{(A8)}$$

where $\mathcal{Y}_\nu$ is the angular momentum/isospin function:

$$\mathcal{Y}_\nu^{M,\tau} = \sum_{\substack{\sigma_a,\sigma_b,\sigma_i \\ \lambda,\tau_a,\tau_b}} \langle s_a\sigma_a, s_b\sigma_b | s_i\sigma_i\rangle \langle s_i\sigma_i, l\lambda | JM\rangle \times \langle t_a\tau_a, t_b\tau_b | t\tau\rangle i^l Y_l^\lambda(\hat{r}_i)\, \chi_a^{\sigma_a} \chi_b^{\sigma_b} \eta_a^{\tau_a} \eta_b^{\tau_b}. \quad \text{(A9)}$$

One can easily argue that the full wave function Ψ must have the same basic angular momentum structure as ψ_i. To see this we write the Bessel function j_l in terms of spherical Hankel functions so that ψ_i becomes a sum of ingoing and outgoing spherical waves, each having well-defined quantum numbers. For example, the ingoing wave in a given angular momentum channel will have the asymptotic form

$$\chi_\nu^{(in)} \rightarrow -\left(\frac{1}{2ik_i r_i}\right) e^{-i(k_i r_i - l\pi/2)}\, \mathcal{Y}_\nu^{M,\tau}. \quad \text{(A10)}$$

We then assume that whatever interactions are present conserve total angular momentum and total isospin. These interactions affect the outgoing waves but do not alter the ingoing wave, and so it follows that the full wave function will be of the form

$$\Psi = 4\pi \sum_\nu \sum_{M,\lambda,\sigma_i,\tau} \langle s_a\sigma_a, s_b\sigma_b | s_i\sigma_i\rangle \langle s_i\sigma_i, l\lambda | JM\rangle \times \langle t_a\tau_a, t_b\tau_b | t\tau\rangle\, \Phi_\nu^{M,\tau} Y_l^{\lambda *}(\hat{k}_i), \quad \text{(A11)}$$

where $\Phi_\nu^{M,\tau}$ is the wave function that evolves from $\chi_\nu^{(in)}$. Although the exact form of Φ_ν may not be known, by our assumptions it must be an eigenfunction of J, M, t, and τ. The formula in Eq. (A11) is our working equation for the expansion of Ψ.

The three-body final state wave function given in Eq. (A5) must also be expanded in terms of angular momentum eigenfunctions. For now we keep the discussion general and allow all three particles to have nonzero spin. Symbolically, the coupling order we adopt is $\{[(s_1,s_2)s_f;l_p]j:[s_3;l_q]j'\}J'$ for the angular momenta and $[(t_1,t_2)t_f;t_3]t'$ for the isospins. The corresponding angular momentum/isospin functions are

$$\mathcal{Y}_\beta^{M',\tau'} = \sum_{\substack{\sigma_1,\sigma_2,\sigma_3,\sigma_f,m,m' \\ \tau_1,\tau_2,\tau_3,\tau_f,\lambda_p,\lambda_q}} \langle s_1\sigma_1, s_2\sigma_2 | s_f\sigma_f\rangle \langle s_f\sigma_f, l_p\lambda_p | jm\rangle \langle s_3\sigma_3, l_q\lambda_q | j'm'\rangle \langle jm, j'm' | J'M'\rangle \langle t_1\tau_1, t_2\tau_2 | t_f\tau_f\rangle \times \langle t_f\tau_f, t_3\tau_3 | t'\tau'\rangle i^{l_p+l_q} Y_{l_p}^{\lambda_p}(\hat{p})\, Y_{l_q}^{\lambda_q}(\hat{q})\, \chi_1^{\sigma_1} \chi_2^{\sigma_2} \chi_3^{\sigma_3} \eta_1^{\tau_1} \eta_2^{\tau_2} \eta_3^{\tau_3}, \quad \text{(A12)}$$

where in this context β is shorthand for the final-state quantum numbers l_p, l_q, j, j', J', s_f, t_f, and t'. The expansion of ψ_f in terms of the $\mathcal{Y}$ functions is

$$\psi_f=(4\pi)^2\sum_\beta \sum_{\substack{M',\sigma_f,\tau_f,\tau' \\ m,m',\lambda_p,\lambda_q}} \langle s_1\sigma_1,s_2\sigma_2|s_f\sigma_f\rangle\langle s_f\sigma_f,l_p\lambda_p|jm\rangle\langle s_3\sigma_3,l_q\lambda_q|j'm'\rangle\langle jm,j'm'|J'M'\rangle\langle t_1\tau_1,t_2\tau_2|t_f\tau_f\rangle$$

$$\times\langle t_f\tau_f,t_3\tau_3|t'\tau'\rangle j_{l_p}(pr)\, j_{l_q}(q\rho)\, Y^{\lambda_p^*}_{l_p}(\hat{p})\, Y^{\lambda_q^*}_{l_q}(\hat{q})\, \mathcal{Y}^{M',\tau'}_\beta . \tag{A13}$$

We may now obtain the partial wave expansion of f_β by substituting Eqs. (A11) and (A13) into Eq. (A4). The result is

$$f^{\sigma_1,\sigma_2,\sigma_3}_{\sigma_a,\sigma_b}=i\left(\frac{2}{\pi\xi}\right)^{1/2}\frac{4E_\beta\mu_1\mu_2}{\hbar^4}\sum_{\substack{\nu,\beta,M,M'\lambda,\sigma_i,\tau,\tau' \\ \sigma_f,m,m',\tau_f,\lambda_p,\lambda_q}} \langle s_a\sigma_a,s_b\sigma_b|s_i\sigma_i\rangle\langle s_i\sigma_i,l\lambda|JM\rangle\langle t_a\tau_a,t_b\tau_b|t\tau\rangle\langle s_1\sigma_1,s_2\sigma_2|s_f\sigma_f\rangle$$

$$\times\langle s_f\sigma_f,l_p\lambda_p|jm\rangle\langle s_3\sigma_3,l_q\lambda_q|j'm'\rangle\langle jm,j'm'|J'M'\rangle\langle t_1\tau_1,t_2\tau_2|t_f\tau_f\rangle\langle t_f\tau_f,t_3\tau_3|t'\tau'\rangle$$

$$\times\langle j_{l_p}(pr)\, j_{l_q}(q\rho)\mathcal{Y}^{M',\tau'}_\beta|V_\beta|\Phi^{M,\tau}_\nu\rangle Y^{\lambda}_{l}{}^*(\hat{k}_i)\, Y^{\lambda_p}_{l_p}(\hat{p})\, Y^{\lambda_q}_{l_q}(\hat{q}). \tag{A14}$$

At this point we can simplify the result by assuming that the interaction potential V_β is a rotational scalar in both ordinary and isospin space. It follows that the matrix elements are nonzero only for $\{J,M,t,\tau\}=\{J',M',t',\tau'\}$. Furthermore, we know from the Wigner-Eckhart theorem that, for a given set of quantum numbers ν and β, the matrix elements are independent of both M and τ. With this in mind we adopt the shorthand notation

$$U_\alpha(\epsilon)=\sqrt{2J+1}\ \langle j_{l_p}(pr)\, j_{l_q}(q\rho)\, \mathcal{Y}^{M,\tau}_\beta|V_\beta|\Phi^{M,\tau}_\nu\rangle, \tag{A15}$$

where, as in Eq. (10), α is shorthand for the full set of initial- and final-state quantum numbers. We see from Eq. (A15) that the matrix element U_α depends explicitly on the momentum parameters p and q. These parameters are constrained by the requirement that the total kinetic energy in the final state must be E_β, and therefore U is effectively a function of the energy sharing parameter ϵ.

To obtain our final expression for the reaction amplitude we adopt the coordinate frame of Fig. 1, in which the z axis is along $\boldsymbol{k}_i$. The result is

$$f^{\sigma_1,\sigma_2,\sigma_3}_{\sigma_a,\sigma_b}=\frac{8i\sqrt{2}}{\sqrt{\xi}}\frac{E_\beta t\mu_1\mu_2}{\hbar^4}\sum_{\substack{\alpha,m,\sigma_i,\tau \\ \sigma_f,m_p,m_q,\tau_f,\lambda_p,\lambda_q}} \langle s_a\sigma_a,s_b\sigma_b|s_i\sigma_i\rangle\langle s_i\sigma_i,l0|JM\rangle\langle t_a\tau_a,t_b\tau_b|t\tau\rangle\langle s_1\sigma_1,s_2\sigma_2|s_f\sigma_f\rangle$$

$$\times\langle s_f\sigma_f,l_p\lambda_p|j_pm_p\rangle\langle s_3\sigma_3,l_q\lambda_q|j_qm_q\rangle\langle j_pm_p,j_qm_q|JM\rangle\langle t_1\tau_1,t_2\tau_2|t_f\tau_f\rangle\langle t_f\tau_f,t_3\tau_3|t\tau\rangle$$

$$\times\left[\frac{2l+1}{2J+1}\right]^{1/2} U_\alpha(\epsilon)\, Y^{\lambda_p}_{l_p}(\hat{p})\, Y^{\lambda_q}_{l_q}(\hat{q}). \tag{A16}$$

Equation (A16) simplifies considerably if we specialize for $pp\to pp\pi^0$. In this case the isospin Clebsch-Gordan coefficients become constant numerical factors. In addition s_3 is zero and $l_q=j_q$. The result is

$$f^{\sigma_1,\sigma_2}_{\sigma_a,\sigma_b}=\frac{8i}{\sqrt{\xi}}\frac{E_\beta t\mu_1\mu_2}{\hbar^4}\sum_{\substack{\alpha,M,\sigma_i,m \\ \lambda_p,\sigma_f,\lambda_q}}\left[\frac{2l+1}{2J+1}\right]^{1/2} \langle s_a\sigma_a,s_b\sigma_b|s_i\sigma_i\rangle\langle s_i\sigma_i,l0|JM\rangle\langle s_1\sigma_1,s_2\sigma_2|s_f\sigma_f\rangle\langle s_f\sigma_f,l_p\lambda_p|jm\rangle$$

$$\times\langle jm,l_q\lambda_q|JM\rangle\, U_\alpha(\epsilon)tY^{\lambda_p}_{l_p}(\hat{p})\, Y^{\lambda_q}_{l_q}(\hat{q}). \tag{A17}$$

2. Cross section and polarization observables

In most respects, the procedure for obtaining the observables from the reaction amplitude is the same as for reactions with two-body final states. In particular one can show that the fivefold differential cross section for a three-body final state is proportional to $f_\beta f^*_\beta$ (averaged over initial spin states and summed over final spin states), where the proportionality constant involves only kinematic factors. For our purposes it is useful to introduce a ''reaction matrix'' M directly proportional to f, with normalization chosen in such a way that the spin-dependent partial cross section $\Delta\sigma$ for reactions leading from initial state σ_a,σ_b to final state σ_1, σ_2, with $\hat{\boldsymbol{p}}$ and $\hat{\mathbf{q}}$ in the intervals $\Delta\Omega_p$ and $\Delta\Omega_q$, and with the energy-sharing parameter ϵ in the interval $\Delta\epsilon$ is given by

$$\Delta\sigma = |M^{\sigma_1\sigma_2}_{\sigma_a\sigma_b}|^2 \Delta\epsilon \Delta\Omega_p \Delta\Omega_q . \tag{A18}$$

For the case in which ϵ is taken to be the pp relative kinetic energy [as in Eq. (21)] the result for M is

$$\begin{aligned} M^{\sigma_1,\sigma_2}_{\sigma_a,\sigma_b} = 8i \left[\frac{\mu_1\mu_2 pq}{v_i \hbar^5}\right]^{1/2} & \sum_{\substack{\alpha,M,\sigma_i,m \\ \lambda_p,\sigma_f,\lambda_q}} \left[\frac{2l+1}{2J+1}\right]^{1/2} \\ & \times \langle s_a\sigma_a, s_b\sigma_b | s_i\sigma_i\rangle \langle s_i\sigma_i, l0 | JM\rangle \\ & \times \langle s_1\sigma_1, s_2\sigma_2 | s_f\sigma_f\rangle \langle s_f\sigma_f, l_p\lambda_p | jm\rangle \\ & \times \langle jm, l_q\lambda_q | JM\rangle \, U_\alpha t Y^{\lambda_p}_{l_p}(\hat{p}) \, Y^{\lambda_q}_{l_q}(\hat{q}), \end{aligned} \tag{A19}$$

where v_i is the relative velocity in the initial state.

The differential cross section and polarization observables may now be obtained directly from the reaction matrix M. In general, the observables O are found by taking the trace of a matrix product, i.e.,

$$O = \mathrm{Tr}[MTM^\dagger], \tag{A20}$$

where T is the appropriate operator. To obtain the unpolarized cross section, the partial cross sections of Eq. (A18) are to be summed over final states and averaged over initial states with the result

$$\sigma_0 = \frac{1}{(2s_a+1)(2s_b+1)} \quad \mathrm{Tr}[MM^\dagger]. \tag{A21}$$

The polarization observables are obtained by using the appropriate spin operators for T in Eq. (A20). For the analyzing powers the operators we want are the Pauli matrices, and the result is

$$\sigma_0 A_{i0} = \frac{1}{(2s_a+1)(2s_b+1)} \ \mathrm{Tr}[M\sigma_i M^\dagger], \tag{A22}$$

where the subscript i can be x, y, or z. In a similar way, the spin correlation parameters are obtained by using for T the direct product of the Pauli matrices for beam and target particles:

$$\sigma_0 A_{ij} = \frac{1}{(2s_a+1)(2s_b+1)} \ \mathrm{Tr}[Mt\sigma^{(b)}_i \otimes \sigma^{(t)}_j t M^\dagger]. \tag{A23}$$

Obtaining the partial-wave expansions is simplified considerably if one introduces spherical tensor spin operators to use in place of the Cartesian spin operators that appear in Eqs. (A22) and (A23). The new operators transform under rotations like the spherical harmonics and are defined, for each particle, by the equations

$$\tau_{00} = I,$$

$$\tau_{10} = \sigma_z,$$

$$\tau_{1\pm1} = \mp \frac{1}{\sqrt{2}} (\sigma_x \pm i\sigma_y), \tag{A24}$$

where I is the 2×2 unit matrix. Associated with these operators, there is corresponding set of ''spherical tensor'' polarization observables [47]

$$T_{k_1q_1,k_2q_2} = \frac{1}{(2s_a+1)(2s_b+1)} \ \mathrm{Tr}[M\tau^{(b)}_{k_1q_1} \otimes \tau^{(t)}_{k_2q_2} M^\dagger]. \tag{A25}$$

From the definitions given above, it is straightforward to find simple relationships between the Cartesian analyzing powers and spin correlation coefficients and the spherical tensor observables. The relevant formulas are

$$\begin{aligned} \sigma_0 &= T_{00,00}, \\ \sigma_0 A_{y0} &= -\sqrt{2}\,\mathrm{Im}[T_{11,00}], \\ \sigma_0 A_{z0} &= T_{10,00}, \\ \sigma_0 A_{zz} &= T_{10,10}, \\ \sigma_0 A_\Sigma &= -2\,\mathrm{Re}[T_{11,1-1}], \\ \sigma_0 A_\Delta &= 2\,\mathrm{Re}[T_{11,11}], \\ \sigma_0 A_{xz} &= -\sqrt{2}\,\mathrm{Re}[T_{11,10}], \\ \sigma_0 A_\Xi &= 2\,\mathrm{Im}[T_{11,1-1}]. \end{aligned} \tag{A26}$$

The introduction of the spherical tensor spin operators leads to a compact, general formula for the partial-wave expansion of the observables. The simplification comes from the fact that the spin operators of Eq. (A24) can be represented in angular momentum language:

$$\langle\sigma|\tau_{kq}|\sigma'\rangle = (-)^{s-\sigma'} \sqrt{2s+1} \langle s\sigma, s-\sigma'|kq\rangle. \tag{A27}$$

To obtain the partial-wave expansion formula we now substitute this expression, along with Eq. (A19) for M, into Eq. (A25). The angular dependence of the observables is expressed as an expansion in terms of bipolar harmonics:

$$B^\Lambda_{L_p,L_q;L}(\hat{p},\hat{q}) = \sum_{\Lambda_p,\Lambda_q} \langle L_p\Lambda_p, L_q\,\Lambda_q | LQ\rangle \, Y^{\Lambda_p}_{L_p}(\hat{p}) \, Y^{\Lambda_q}_{L_q}(\hat{q}). \tag{A28}$$

After carrying out an angular momentum reduction that eliminates the sums over the magnetic quantum numbers we obtain the result

$$\begin{aligned} T_{k_1q_1,k_2q_2} = \frac{1}{(2s_a+1)(2s_b+1)} & \left(\frac{16\,\mu_1\,\mu_2\,p\,q}{v_i\,\pi\,\hbar^5}\right) \\ & \times \sum_{L_p,L_q,L} \left[\sum_{\alpha,\alpha'} C^{\alpha,\alpha';\kappa}_{L_p,L_q;L} \, U_\alpha(\epsilon) \, U^*_{\alpha'}(\epsilon)\right] \\ & \times B^Q_{L_p,L_q;L}(\hat{p},\hat{q}), \end{aligned} \tag{A29}$$

where the label κ is shorthand for the indices $k_1 q_1, k_2 q_2$ and where $Q = q_1 + q_2$.

Equation (A29) represents our central result for the partial-wave expansion of the cross section and polarization observables. Each observable has a set of allowed angular dependences, $B^{Q}_{L_p,L_q;L}(\hat{p},\hat{q})$, and the factor inside the square brackets gives the expansion coefficient. Each of these coefficients is a sum of terms involving an angular momentum coupling coefficient C and a bilinear product of matrix elements U_α. The selection rules that determine which partial-wave combinations contribute to a given angular function are contained in the C coefficients.

The angular momentum coefficients are given by the following expression:

$$
\begin{aligned}
C^{\alpha,\alpha';\kappa}_{L_p,L_q;L} = (-)^{l'_p+l'_q+l+s_i-J-s'_i+J'}\,\delta_{s_f,s'_f}\sum_{I,K}\,&[(2s_a+1)(2s_b+1)(2k_1+1)(2k_2+1)(2K+1)\times(2I+1)(2s_i+1)(2s'_i+1)\\
&\times(2l+1)(2l'+1)(2l_p+1)(2l'_p+1)(2l_q+1)(2l'_q+1)(2j+1)(2j'+1)(2J+1)(2J'+1)]^{1/2}\\
&\times\langle l0,l'0|I0\rangle\langle I0,KQ|LQ\rangle\langle l_p0,l'_p0|L_p0\rangle\langle l_q0,l'_q0|L_q0\rangle\langle k_1q_1,k_2q_2|KQ\rangle\, W(j,s_f,L_p,l'_p;l_p,j')
\begin{Bmatrix} s_i & J & l \\ s'_i & J' & l' \\ K & L & I \end{Bmatrix}\\
&\times\begin{Bmatrix} j & l_q & J \\ j' & l'_q & J' \\ L_p & L_q & L \end{Bmatrix}\begin{Bmatrix} s_a & s_a & k_1 \\ s_b & s_b & k_2 \\ s_i & s'_i & K \end{Bmatrix}. \qquad \text{(A30)}
\end{aligned}
$$

This equation differs from the analogous formula given in Ref. [9] in two respects. First of all the Clebsch-Gordan coefficient $\langle l0,l'0|I0\rangle$ was inadvertently omitted in Ref. [9]. Second, we have changed the coupling order for the angular momenta in the initial state [see Eqs. (A8) and (A9)] and this results in additional phase factors in C.

Although the expression given in Eq. (A30) is fairly complex, the coefficients are easily evaluated since computer codes for calculating the Clebsch-Gordan, Racah, and $9j$ symbols are readily available.

The expansion formulas given in Eq. (11) are obtained most readily by substituting Eq. (A28) into Eq. (A29) to obtain

$$
\begin{aligned}
T_{k_1q_1,k_2q_2} = &\frac{1}{(2s_a+1)(2s_b+1)}\left(\frac{16\,\mu_1\,\mu_2\,p\,q}{v_i\,\pi\,\hbar^5}\right)\\
&\times\sum_{L_p,L_q,\mu}\left[\sum_{\alpha,\alpha'} X^{\alpha,\alpha';\kappa}_{L_p,L_q,\mu}\,U_\alpha(\epsilon)\,U^*_{\alpha'}(\epsilon)\right]\\
&\times Y^{\mu}_{L_p}(\hat{p})\,Y^{Q-\mu}_{L_q}(\hat{q}), \qquad \text{(A31)}
\end{aligned}
$$

where the coefficients X are given by

$$
X^{\alpha,\alpha';\kappa}_{L_p,L_q,\mu} = \sum_L \langle L_p\mu, L_q\,Q-\mu|LQ\rangle\, C^{\alpha,\alpha';\kappa}_{L_p,L_q;L}. \qquad \text{(A32)}
$$

Equations (11) are then obtained by using Eq. (A31) in conjunction with Eqs. (A30) and (A32) assuming that only the partial waves of Table I contribute and that terms quadratic in **Sd** or **Ds** are negligible. In general, one finds that only a few distinct angular functions are allowed for each observable. The constraints, which arise from conservation laws and the antisymmetrization requirements, can be seen by inspecting Eq. (A30).

The first constraint comes from the δ_{s_f,s'_f} factor. For $pp \to pp\pi^0$, s_f is the pp total spin quantum number. Since we have only antisymmetric pp states, the conclusion is that there will be no interference between even l_p and odd l_p partial waves.

The next constraint is on the allowed values of L_p. This constraint comes from the Clebsch-Gordan coefficients $\langle l_p0,l'_p0|L_p0\rangle$ which requires that l_p l'_p and L_p satisfy the triangle inequality and also that $l_p+l'_p+L_p$ be even. There are analogous constraints on L_q. Thus, for example, interference between Ps and Pp may give rise to angular distributions with $L_p=0$ and 2 and with $L_q=1$. For the conditions we assume, the angular distributions involve no spherical harmonics of degree greater than $L=2$.

One can easily demonstrate from Eq. (A30) that X coefficients are either symmetric or antisymmetric under the interchange of α and α':

$$
X^{\alpha,\alpha';\kappa}_{L_p,L_q,\mu} = (-)^{k_1+k_2} X^{\alpha',\alpha;\kappa}_{L_p,L_q,\mu}. \qquad \text{(A33)}
$$

This means that the unpolarized cross section and the spin correlation parameters depend only on $\mathrm{Re}[U_\alpha U^*_{\alpha'}]$ whereas the analyzing powers depend only on $\mathrm{Im}[U_\alpha U^*_{\alpha'}]$. One consequence is that the factor inside the square brackets in Eq. (A29) is either purely real or purely imaginary. From this it follows that a given observable will depend either on $\mathrm{Re}[Y^{\mu}_{L_p}(\hat{p})\,Y^{Q-\mu}_{L_q}(\hat{q})]$ or on $\mathrm{Im}[Y^{\mu}_{L_p}(\hat{p})\,Y^{Q-\mu}_{L_q}(\hat{q})]$, and as a

result the ϕ dependences of the allowed angular distributions are relatively simple. In particular we see that $\sigma_0 A_{z0}$ and $\sigma_0 A_{\Xi}$ (both of which have $Q=0$) go as $\sin[\mu(\phi_p-\phi_q)]$, while the remaining observables go as $\cos[\mu(\phi_p-\phi_q)+Q\phi_q]$.

The formalism outlined in this appendix leads to a number of additional useful results that are described in the main text and in other publications.

[1] J. Marshall, L. Marshall, V.A. Nedzel, and S.D. Warshaw, Phys. Rev. **88**, 275 (1952); J.W. Mather, and E.A. Martinelli, *ibid.* **92**, 780 (1953).

[2] C.M.G. Lattes, G. Occhialini, and C.F. Powell, Nature (London) **160**, 453 (1947).

[3] H. Yukawa, Proc. Phys. Math. Soc. Jpn. **17**, 48 (1935).

[4] R.E. Pollock, Annu. Rev. Nucl. Part. Sci. **41**, 357 (1991).

[5] H.O. Meyer, C. Horowitz, H. Nann, P.V. Pancella, S.F. Pate, R.E. Pollock, B.v. Przewoski, T. Rinkel, M.A. Ross, and F. Sperisen, Nucl. Phys. **A539**, 633 (1992).

[6] G. Rappenecker *et al.*, Nucl. Phys. **A590**, 763 (1995).

[7] S. Stanislaus, D. Horvath, D.F. Measday, A.J. Noble, and M. Salomon, Phys. Rev. C **44**, 2287 (1991).

[8] G.G. Ohlsen, Rep. Prog. Phys. **35**, 717 (1972).

[9] L.D. Knutson, in *Nuclear Physics at Storage Rings*, edited by H.O. Meyer and P. Schwandt, AIP Conf. Proc. No. 512 (AIP, Melville, NY, 2000), p. 177.

[10] J. Złomańczuk *et al.*, Phys. Lett. B **436**, 251 (1998).

[11] H.O. Meyer *et al.*, Phys. Rev. Lett. **83**, 5439 (1999).

[12] T. Rinckel *et al.*, Nucl. Instrum. Methods Phys. Res. A **439**, 117 (2000).

[13] T. Wise, A.D. Roberts, and W. Haeberli, Nucl. Instrum. Methods Phys. Res. A **336**, 410 (1993).

[14] F. Rathmann *et al.*, Phys. Rev. C **58**, 658 (1998).

[15] B.v. Przewoski *et al.*, Phys. Rev. C **58**, 1897 (1998).

[16] W. Haeberli and B.R. Holstein, in *Symmetries and Fundamental Interactions in Nuclei*, edited by W.C. Haxton and E.M. Henley (World Scientific, Singapore, 1995), p. 17.

[17] H.O. Meyer *et al.*, Phys. Lett. B **480**, 7 (2000).

[18] M.G. Bachman *et al.*, Phys. Rev. C **52**, 495 (1995).

[19] E.A. George, J. Frandy, M.K. Smith, Y. Zhou, L.D. Knutson, J. Golak, H. Witala, W. Glöckle, and D. Hüber, Phys. Rev. C **54**, 1523 (1996).

[20] K.M. Watson, Phys. Rev. **88**, 1163 (1952).

[21] B.J. Morton, E.E. Gross, E.V. Hungerford, J.J. Malanify, and A. Zucker, Phys. Rev. **169**, 825 (1968).

[22] H.P. Noyes, Annu. Rev. Nucl. Sci. **22**, 465 (1972).

[23] C. Hanhart and K. Nakayama, Phys. Lett. B **454**, 176 (1999).

[24] H. Garcilazo and T. Mizutani, *πNN Systems* (World Scientific, Singapore, 1990).

[25] G.A. Miller and P. Sauer, Phys. Rev. C **44**, R1725 (1991).

[26] J.A. Niskanen, Phys. Lett. B **289**, 227 (1992).

[27] T.-S.H. Lee and D.O. Riska, Phys. Rev. Lett. **70**, 2237 (1993).

[28] C.J. Horowitz, H.O. Meyer, and D.K. Griegel, Phys. Rev. C **49**, 1337 (1994).

[29] E. Hernandez and E. Oset, Phys. Lett. B **350**, 158 (1995).

[30] C. Hanhart, J. Haidenbauer, O. Krehl, and J. Speth, Phys. Lett. B **444**, 25 (1998).

[31] B.-Y. Park, F. Myhrer, J.R. Morones, T. Meissner, and K. Kubodera, Phys. Rev. C **53**, 1519 (1996).

[32] T.D. Cohen, J.L. Friar, G.A. Miller, and U.v. Kolk, Phys. Rev. C **53**, 2661 (1996).

[33] J. Adam, A. Stadler, M.T. Peña, and F. Gross, Phys. Lett. B **407**, 97 (1997).

[34] U. Van Kolck, G.A. Miller, and D.O. Riska, Phys. Lett. B **388**, 679 (1996).

[35] M.T. Peña, D.O. Riska, and A. Stadler, Phys. Rev. C **60**, 045201 (1999).

[36] E. Gedalin, A. Moalem, and L. Razdolskaya, Phys. Rev. C **60**, 031001 (1999).

[37] T. Sato, T.-S.H. Lee, F. Myhrer, and K. Kubodera, Phys. Rev. C **56**, 1246 (1997).

[38] E. Gedalin, A. Moalem, and L. Razdolskaya, Nucl. Phys. **A652**, 287 (1999).

[39] A. Engel, R. Shyam, U. Mosel, and A.K. Dutt-Mazumder, Nucl. Phys. **A603**, 387 (1996).

[40] K. Tamura, Y. Maeda, and N. Matsuoka, in *Proceedings of the 15th International Conference On Particles and Nuclei*, Uppsala, Sweden, edited by G. Fäldt, B. Höistad, and S. Kullander, [Nucl. Phys. **A663&664**, 456c (2000)].

[41] C. Hanhart, J. Haidenbauer, and J. Speth, Acta Phys. Pol. B **29**, 3047 (1998).

[42] C. Hanhart, J. Haidenbauer, O. Krehl, and J. Speth, Phys. Rev. C **61**, 064008 (2000).

[43] J. Haidenbauer, Ch. Hanhart, and J. Speth, Acta Phys. Pol. B **27**, 2893 (1996).

[44] N. Austern, *Direct Nuclear Reaction Theories* (Wiley, New York, 1970).

[45] It appears that the Green's function given in Eq. (1.38) of Ref. [44] contains a typographical error. The dependence on the masses should be M_1M_2 rather than $(M_1M_2)^{1/2}$. See E. Gerjuoy, Ann. Phys. (N.Y.) **5**, 58 (1958).

[46] M.E. Rose, *Elementary Theory of Angular Momentum* (Wiley, New York, 1957).

[47] S.E. Darden, in *Proceedings of the International Conference on Polarication Phenomena in Nuclear Physics*, edited by H. H. Barschall and W. Haeberli (University of Wisconsin Press, Madison, 1971), p. 39.